Probabilistic modeling of the size effect and scatter in High Cycle Fatigue using a Monte-Carlo approach: role of the defect population in cast aluminum alloys

Driss El Khoukhi, Franck Morel, Nicolas Saintier, Daniel Bellett, Pierre Osmond, Viet-Duc Le

Probabilistic modeling of the size effect and scatter in High Cycle Fatigue using a Monte-Carlo approach: role of the defect population in cast aluminum alloys

Driss EL KHOUKHI[1, 2, 3,*], Franck MOREL[1], Nicolas SAINTIER[2], Daniel BELLETT[1], Pierre OSMOND[3], Viet-Duc LE[1]

[1]LAMPA, Arts et Métiers Institute of Technology, 49 035 Angers, Cedex, France
[2]I2M, Arts et Métiers Institute of Technology, 33170 Talence, Cedex, France
[3]Groupe PSA, 78955 Carrières-sous-Poissy, Cedex, France

Abstract

In this study, a probabilistic model based on Monte-Carlo theory is applied to predict the fatigue behavior of cast aluminum alloys. The objective of the proposed approach is to investigate the effect of porosity (i.e. the defect size distribution and spatial density) on the fatigue strength and its associated scatter for uniaxial fatigue loads with the load ratio R=0.1. The proposed model is applied to two cast aluminum alloys with very different defect characteristics. The results for these two alloys confirm that the model can be used to predict the average fatigue strength with a relative error less than 5%. It also accurately reproduces the experimentally observed trends concerning the scatter in fatigue strength. The scatter is underestimated but is of the same order of magnitude as the experimental values. It is believed that this is because the proposed model considers that the porosity is the only source of scatter. It is demonstrated that the model is well adapted for the prediction of the volume or scale effect in fatigue. This approach can also be used to estimate the Representative Volume Element in Fatigue for cast aluminum alloys.

Keywords: High cycle fatigue, Cast aluminum alloys, Probabilistic model, Representative Volume Element (RVE), Size effect in fatigue, Highly stressed volume, Scatter in fatigue strength, Casting defect population

1. Introduction

Many experimental studies have highlighted the dependence of the fatigue strength on the size of the tested sample (Kloos et al. 1981) and the presence of a stress gradient (Papadopoulos and Panoskaltsis 1996). The size effect corresponds to the decrease in the fatigue strength observed when the specimen size is increased. It is generally explained by an increase in the probability of encountering larger defects in larger loaded volumes, which leads to a lower fatigue strength. Other authors have shown that the presence of a stress gradient has a beneficial effect on the fatigue resistance by comparing the results of different loading conditions with and without stress gradients (Morel and Palin-luc 2002; Gaenser 2008).

(Kuguel 1961) was the first to introduce the notion of a Highly Stressed Volume (HSV) which can be used to conjointly analyze both the stress gradient and the size effects. Since then, the HSV approach has been commonly used for this purpose by many authors (Kuguel 1961; Sonsino and Fischer 2005; Morel and Palin-luc 2002; Yang Ai et al. 2019). For any given geometry, the Highly Stressed Volume is selected as the regions subjected to more than n% of the maximum stress. This percentage is assumed to be 95% by (Kuguel 1961), 90% by (Sonsino and Fischer 2005) and 80% by El Khoukhi in the present work and in previous publications (El Khoukhi et al. 2019). It has been demonstrated that this approach yields accurate predictions for the fatigue behavior of both the notched and smooth specimens (Y. Ai et al. 2019; Yang Ai et al. 2019; Zhu et al. 2018).

Experimental results indicate that, in terms of the local stress at a notch-tip (i.e. the hotspot stress), a notched specimen can endure higher stresses in comparison with smooth specimens due to the smaller Highly Stressed Volume (Sun and Song 2018). Furthermore, other experimental works have shown that the fatigue strength does not decrease indefinitely as the Highly Stressed Volume increases. This

indicates the presence of a Representative Volume Element (RVE) in fatigue above which the fatigue strength is constant and below which a volume effect is observed.

In addition, a great deal of experimental work has shown that cast aluminum alloys have a high degree of scatter associated with their fatigue strength (El Khoukhi et al. 2018; Romano et al. 2019; El Khoukhi et al. 2019). It is generally accepted that the important parameters controlling the fatigue strength of a specimen are a combination of (a) the size of the largest defects in the HSV and (b) the distance between the largest defects and the free surface of the specimen (Murakami 1991 ; Murakami and Endo 1994). The variation of these parameters in individual specimens leads to a variation in the fatigue strengths of the batch. This explains the high scatter in the fatigue strength of this type of materials for which the fatigue strength is predominately controlled by defects. Undoubtedly, other factors also exist and influence the scatter in the fatigue strength (i.e. experimental error, surface roughness, residual stresses, heat treatment, microstructure etc.). However, it is proposed here that the dominate factors are related to the defect characteristics of the material. Furthermore, many works have shown that the scatter of the fatigue strength for the large samples is smaller than that for the smaller ones (El Khoukhi et al. 2019 ; Yi et al. 2007).

From an industrial point of view, taking into account these two phenomena (the size effect and scatter) is crucial to the structural integrity assessment and reliability evaluation of engineering components.

In order to gain insight into these phenomena, extensive experimental work is usually required. Many specimens with different sizes and shapes should be tested in order to investigate the decrease in fatigue strength versus the Fatigue Active Volume and to estimate the RVE. Also, in order to assess the scatter in the fatigue strength with a high level of confidence, more than 50 tests per batch is needed (Pollak 2005). Furthermore, the results obtained on the standard sized specimens should be re-evaluated to make them applicable to real structures. Due to the time and cost of a full-scale testing program like this, the use of probabilistic models to predict the fatigue behavior has become more common in recent years. In general, deterministic analyses are considered insufficient. In most deterministic procedures (Devlukia et al. 1997), to ensure the integrity of components, the concept of a safety factor is normally used. However, these empirical coefficients do not explain the origin of the dispersion, which limit the optimization of the component of interest. Thus, probabilistic approaches are more useful and are capable of capturing the aforementioned features of the fatigue phenomenon. In addition, the relationship between small size specimens and full-scale components can be established easily by probabilistic modeling of the size effect.

The Weibull Weakest-Link theory (Weibull 1939; Freudenthal and Gough 1946) is the tool most commonly used to interpret the statistical size effect, i.e. to describe how the probability of failure under a given stress depends on the size or volume of loaded material. The main shortcoming of Weibull's original formulation is that fracture is assumed to occur from the largest flaw. However, experience shows that it is not systematically the largest flaw contained in the structure that leads to failure. A smaller flaw close to the surface can be sometimes more critical.

In order to correct this shortcoming, a combination of the Weibull theory and the Highly Stressed Volume approach is usually used (Yang Ai et al. 2019). In this approach, only the active volume of the specimen is considered. The Weibull distribution supported by experimental data has been used for the statistical analysis of the fatigue strength and to investigate the statistical size effect by many authors. For example, (Shirani and Härkegård 2011) investigated the size effect on the fatigue strength of EN-GJS-400-18-LT ductile casting irons and (Rafsanjani and Sørensen 2015) presented a probabilistic model for fatigue failure probability estimation.

To summarize, the characteristics of the defect population (i.e. the defect size distribution and the spatial defect density) of the material are the keys factors controlling certain aspects of the fatigue behavior, in particular the size effect, the scatter and the size of the RVE.

From this postulate, a probabilistic model using a Monte-Carlo approach is proposed in this article to examine how specific changes to the nature of the porosity population, in particular the average pore size and the pore spatial density, affect the fatigue strength and its scatter. These two parameters are estimated by changing the "virtual" volume of the specimen in order to understand the size effect. The proposed model uses the HSV concept in combination with Monte-Carlo sampling and aims to:

- Predict the sensitivity of two cast aluminum alloys to the size effect (with or without the presence of a stress gradient).
- Provide an estimation of the RVE for both alloys.
- Provide an estimation of the scatter in fatigue strength for both alloys.

The current work is organized as follows: (i) a general description is given for the proposed probabilistic approach for fatigue failure analysis, followed by a description of each step of the modeling approach. (ii) The results of the model applied to two very different, but fictive defect populations are presented. The influence of the defect size distribution on the fatigue strength and its scatter is investigated. Then (iii) the influence of the defect spatial density is presented, and (iv) the model is applied to two cast aluminum alloys. The model is validated for these alloys via comparison with experimental data. Finally, (v) the approach is used to study the effect of the number of tests used in the experimental protocol on the accuracy of the estimated fatigue strength.

2. Proposed probabilistic approach

The global approach proposed to study the probabilistic fatigue behavior of cast aluminum alloys is presented in the flowchart shown in Figure 1.

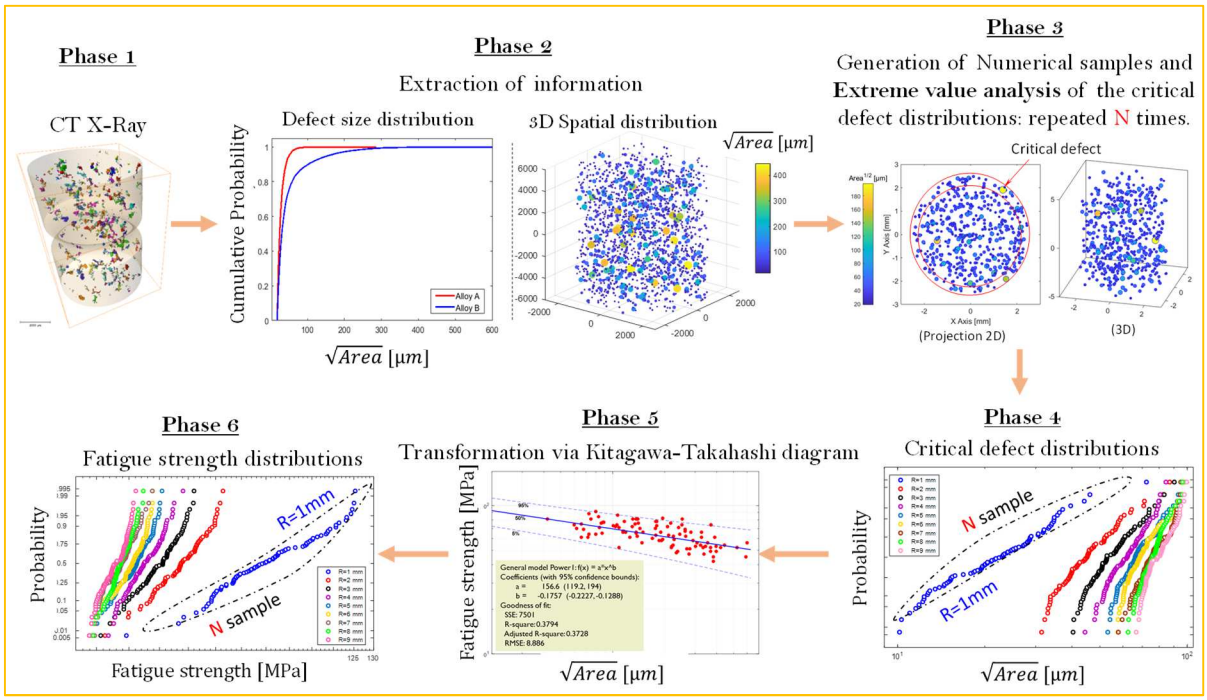

Figure 1 : Flow diagram for the proposed probabilistic approach showing the main phases used to predict the fatigue strength.

The global approach is based on the Monte-Carlo method. Each step is explained in detail in the following section.

2.1. Porosity characterization (Phase 1 and 2)

In phases 1 and 2, the defect population in the material is characterized using X-Ray micro-tomography. From the scanned volume, the defect size distribution and the location of individual

defects can be determined in 3D space. The defect size is then characterized in terms of the equivalent Murakami parameter $\sqrt{\text{Area}}_{\text{eq}}$ of the defect (Murakami 1991). The relationship between the pore volume obtained by tomography and its equivalent square root value of the projected area is given by (eq. 1). This relationship is obtained by assuming the pores have a spherical shape.

$$\sqrt{Area}_{eq} = \pi^{1/6} \left(\frac{3V_{pore}}{4}\right)^{1/3} \quad \text{(eq. 1)}$$

where V_{pore} is the pore volume.

This approximation makes it possible to compare the pore sizes obtained by the CT scans and those measured on the fatigue failure surfaces.

Point process theory can be used to characterize the defect spatial distribution. The natural defect population can then be numerically reproduced to create synthetic materials. Greater details are given in a work under submission (El Khoukhi et al. 2020).

2.2. **Generation of numerical synthetic materials (Phase 3)**

In phase 3, synthetic materials that mimic key macroscale features of the defect population in terms of size and 3D spatial distribution are generated.

The experimental defect size distribution can be approximated by fitting a standard statistical distribution, such as the normal, log-normal or Weibull distributions. The choice of the distribution and the identification of the most suitable parameters are discussed in the work under submission referenced as (El Khoukhi et al., 2020) and summarized in the following sections. This distribution is then used to generate the defect sizes for the synthetic materials.

If the spatial distribution of the natural defects is unknown or presents a small degree of clustering, the Poisson process can be used to generate the 3D positions of the synthetic defects. In this work Point Process Theory has been used in order to characterize the spatial distribution of the natural defects present in the material (El Khoukhi et al. 2020). It has been shown that the natural defect populations do not present a high level of clustering. This is especially true for the largest defects which are the most likely to control the fatigue behavior. Hence, it is concluded that the Poisson Process is suitable to approximate the spatial distribution of the pores present in the investigated alloys. In this case, the density ρ that defines the number of pores per unit volume [mm^{-3}] is important for the generation of the pores in the numerical samples and corresponds to the average number of pores per unit volume. The number of points in a sample volume follows a Poisson distribution (eq. 2) with the parameter ρ|V|, where |V| is the volume of the sample:

$$P\{N(V) = k\} = \frac{(\rho|V|)^k}{k!} e^{-\rho|V|} \quad \text{(eq. 2)}$$

Therefore, when considering a numerical sample of volume V generated from a material with a pore density of ρ, the average number of pores N_t contained in the numerical sample is given by (eq. 3):

$$N_t = \rho \times V \quad \text{(eq. 3)}$$

An example of a synthetic material is presented in Figure 5.

2.3. **Extreme value analyses (Phase 3 and 4)**

From phase 3 to phase 4, extreme value analyses are applied. This consists of extracting the most critical defect in the Fatigue Active Volume (FAV). The principle of sampling and the definition of FAV are presented in the following paragraphs.

- **Principle of sampling**

In terms of fatigue behavior, experience shows that the most critical defect in a structure or specimen is usually the largest defect that exists close to the surface (Le et al. 2016; Iben Houria et al. 2015; Serrano-Munoz et al. 2017; Boromei et al. 2010; Mu et al. 2014; Rotella et al. 2017). To take this into account, only the subsurface volume that we called FAV should be considered.

For the definition of the FAV of a sample, first we estimate the Highly Stressed Volume under at least 80% of the maximal principal stress. Then, we take just the subsurface volume of thickness 't' (Figure 3 .d). The thickness 't' of the subsurface layer is a parameter estimated from the defect population and it can be considered a material characteristic. The idea is to define 't' so that the subsurface layer would be thick enough to include even the "largest" critical defect found in the defect population. It is therefore defined as the distance from the furthest point on a critical defect to the free surface observed on the fatigue failure surfaces of the tested samples. The parameter 't' is made equal to the maximum 'Depth' observed in the whole batch. More details on the definition of the FAV are given in (El Khoukhi et al. 2019).

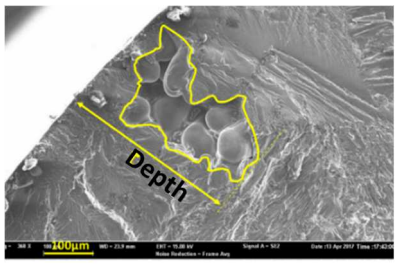

Figure 2:The definition of the 'Depth' of a critical defect.

The use of FAV based on the concept of Highly Stressed Volume is interesting in order to take stress gradient effect into account and it is possible to treat both notched and smooth samples in the same manner.

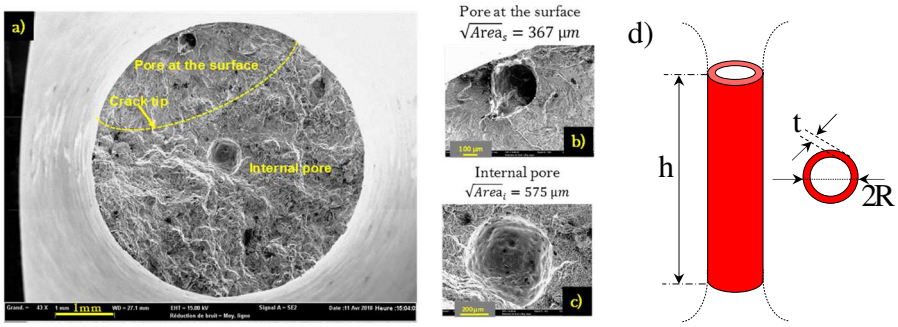

Figure 3: (a) Specimen fatigue failure surface for cast aluminum alloy (AlSi7Mg03 - T7), that has failed at Sa= 55 MPa for Nf=919402 cycles with a stress ratio R=0.1, (a) Macroscopic view, detailed view of (b) surface pore and (c) internal pore. The SEM observations clearly show that the smallest pore close to the surface is responsible for the fatigue failure, (d) representation of FAV in the smooth specimen.

the "Fatigue Active Volume" (Figure 3 .d and Figure 4 .c). The relationship between them is given in (eq. 4).

$$\text{Fatigue Active Volume} = \pi h(2Rt - t^2) \qquad \text{(eq. 4)}$$

In the case of presence of stress gradient such as the notched samples, the FAV is presented in Figure 4. There are two possible cases:

- for the case where the width of the V80% < t, the width of FAV is equal to 't' (FAV > V80%) [Figure 4 .a].

- for the case where the width of the V80% > t, the width of FAV is limit to 't' (FAV < V80%) [Figure 4 .b].

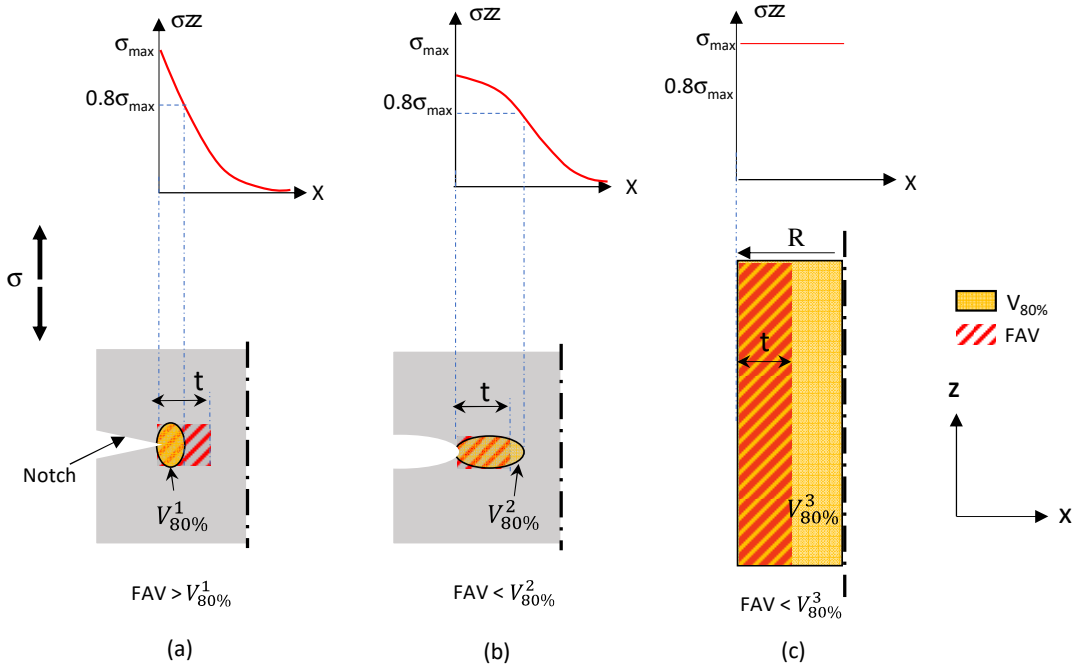

Figure 4: definition of the Fatigue Active Volume (FAV) and the Highly Stressed Volume (V80%) in (a) case of sharp notched samples, (b) case of blunt notched samples, and (c) case of smooth samples.

From the extensive experimental work presented in (El Khoukhi et al. 2019), the thickness of subsurface layer for the studied alloys was defined as 0.5 mm for the alloy A (AlSi7Cu05Mg03 - T7) and 0.65 mm for the alloy B (AlSi7Mg03 - T7). These values will be used for the application of the model to these alloys.

In the numerical study, the critical defect is defined as the largest defect contained in the FAV (see Figure 5).

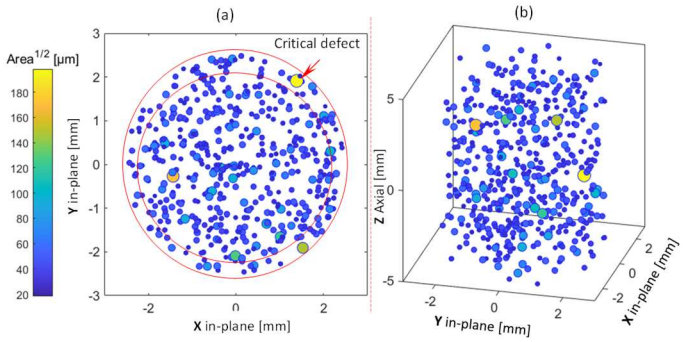

Figure 5: Schematic representation of a numerical sample and its critical defect (R=2.5 mm, h=10 mm) (a) is the projected view (plane X-Y) and (b) is the 3D representation.

By repeating N times the generation of the numerical sample and extracting the critical defect in each iteration, a distribution of N critical defects can be obtained. In general, this distribution follows the lognormal probability function (El Khoukhi et al. 2019). Physically, the N repetitions correspond to the number of samples. The same distribution can be compared to the distribution of critical defects

established by measuring the size of critical defects from fractography analyses of real fatigue test specimens.

- **Relationship between the critical defects and the fatigue strength (phase 5)**

It is well known that the fatigue strength decreases when the size of the critical defect increases. This relationship is described in the Kitagawa-Takahashi diagram, shown schematically in Figure 6. The objective of phase 5 is to obtain the distribution of the fatigue strength from the distribution of the critical defects. In this article, the fatigue strength is defined as the stress amplitude that the material can withstand 2 millions cycles, with a stress ratio of 0.1, without fatigue failure.

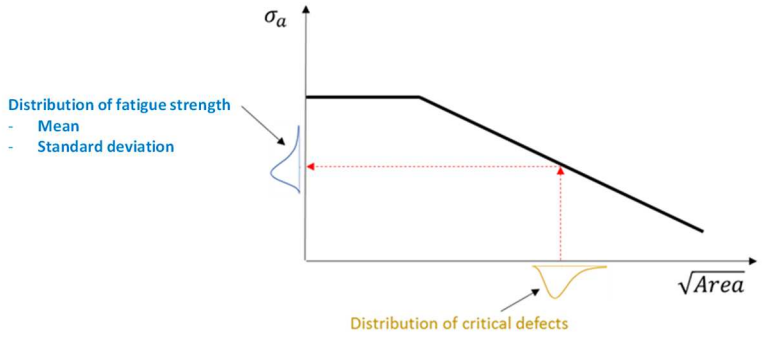

Figure 6: relationship between the critical defects and the fatigue strength

The transformation from the distribution of the critical defects, obtained in phase 4, to the distribution of the fatigue strength can be done using an equation established from the experimental data shown in Figure 7 called the Kitagawa-Takahashi diagram. It presents the local fatigue strength as a function of the critical defect size measured on the fatigue failure surface. As discussed in (El Khoukhi et al. 2019), the local fatigue strength (or the fatigue strength expressed in terms of the "hotspot" stress) is expressed as $K_t\sigma_D$, where σ_D is the nominal stress calculated by dividing the applied force by the net section of the notched specimens and K_t is the stress concentration factor. In addition, σ_D is determined at 2 million cycles, via interpolation using eq. 5, proposed by (Lanning et al., 2005) and estimated using the data obtained by the staircase method with a step of 5 MPa. The run-out specimens were retested until failure at higher load levels.

$$\sigma_D(N = 2 \times 10^6 cycles) = \sigma_{n-1} + (\sigma_n - \sigma_{n-1}) \times \frac{N_f}{2\times10^6} \qquad \text{(eq. 5)}$$

In eq. 5, σ_{n-1} is the stress amplitude value of the loading block prior to the block where failure occurs. σ_n is the stress level of the final block of cycles during which failure occurs, and N_f is the number of cycles to failure in the final loading block. For the specimens that fail at the first stress level (σ_n) the existence of a fictive level (σ_{n-1}) is assumed.

In references (Engelke and Esderts 2018; Lipp et al., 2013), it was shown that there is good correlation between the fatigue strength expressed as $K_t\sigma_D$ and the highly stressed volume. It is important to note also that by defining the fatigue strength in terms of the "hotspot" stress ($K_t\sigma_D$) it is simple to compare notched samples (Kt=1.68) and smooth samples (Kt=1).

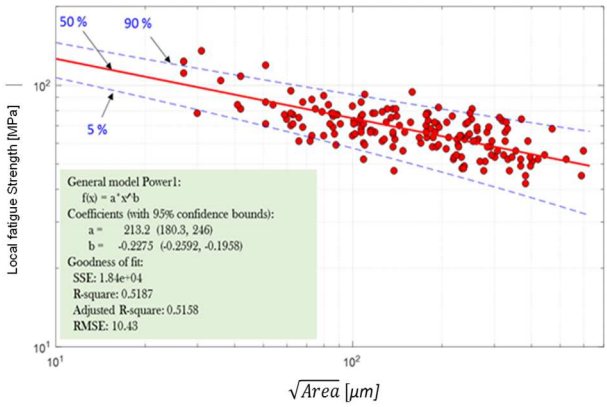

Figure 7: Diagram of Kitagawa-Takahashi for R=0.1 see (El Khoukhi et al. 2019)

When dealing with a new material, there are several ways to obtain the dependence of the fatigue strength to the defect size, such as the Murakami empirical approach (Murakami and Endo 1994) or the El-Haddad equation (El Haddad et al. 1979).

- **Detailed description of the probabilistic approach for the case of cylindrical numerical specimens**

As previously mentioned, the numerical samples generated N times make it possible to establish a distribution of critical defects that could be compared to the experimental distribution of critical defects measured on the fatigue failure surfaces of real specimens. The Monte-Carlo procedure used for these simulations is explained and summarized in the flowchart in Figure 8.

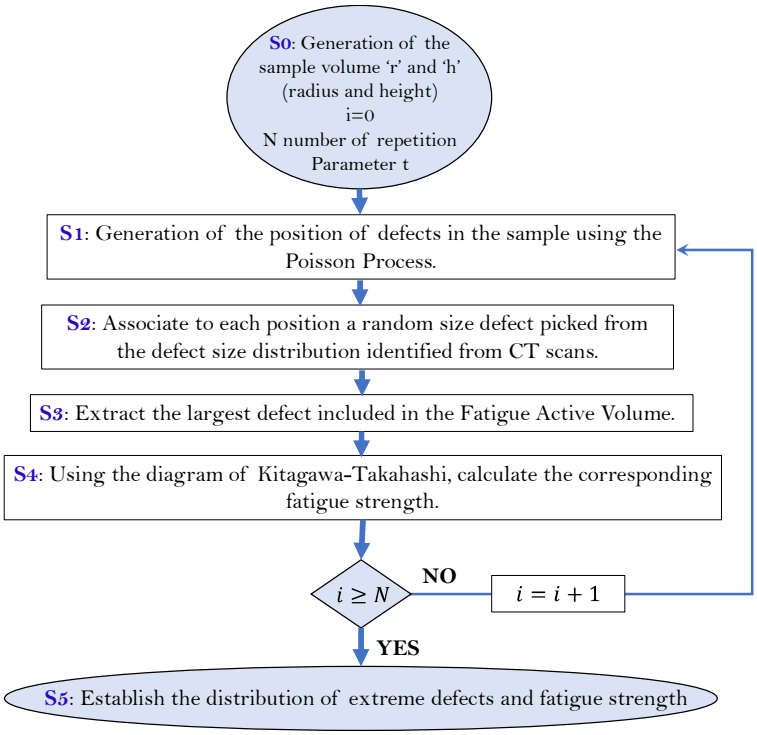

Figure 8: Flow chart for the probabilistic determination of critical defect and fatigue strength distributions. The algorithm was implemented in Matlab.

In the flow chart shown in Figure 8, the first step **(S0),** which corresponds to **'Phase 3'** in Figure 1, consists of defining the sample volume by fixing its radius 'r' and its height 'h'. At the same time, the

number of repetitions 'N' corresponding to the number of samples in the batch is defined. The parameter 'i' corresponds to the sample's number.

After defining the sample volume, the next step **(S1)** is to generate the defects within the volume. The 3D defect positions are generated using the Poisson process. In step **(S2),** for each position, a defect size is randomly selected from the defect size distribution, which was identified from the CT scans. This corresponds to **'Phase 2'** in Figure 1. *Note that other "fictive" distributions could be used to study the effect of different parameters of the defect population, such as the average defect size and its standard deviation*. Following the numerical generation of the sample, the most critical defect is extracted **(S3)**. The critical defect is defined as the largest defect in the Fatigue Active Volume and shown in **'Phase 3'** (Figure 1).

After extraction of the critical defect, the Kitagawa-Takahashi diagram shown in '**Phase 5'** of Figure 1, is used to calculate the corresponding fatigue strength for the sample **(S4).**

The preceding steps (**S1** to **S4**) are repeated N times, which makes it possible to establish the critical defect distribution (see **'Phase 4'** in Figure 1) and the fatigue strength distribution (see **'Phase 6'** in Figure 1) corresponding to the sample volume. This is step **S5**.

Finally, descriptive statistical analyses are applied to investigate the evolution of the average and the standard deviation of the resulting distributions.

To summarize, to set-up the probabilistic modeling algorithm, the following parameters must be defined:

- The volume of the sample, via its radius *r* (or diameter) and height *h*.
- the definition of the Fatigue Active Volume via the 't' thickness parameter.
- The pore spatial density ρ. This parameter is needed for the generation of the 3D positions of the pores using the Poisson process.
- The defect size distribution parameters (for example, the location, shape and scale parameters of the Weibull distribution)
- The number of repetitions N (number of samples in the batch) with the same volume.

Many phenomena can be investigated using this algorithm.

- ✓ The volume effect in fatigue: this phenomenon can be investigated by changing the volume of the numerical samples (either the radius, the height or both) and fixing the other parameters ρ, N and the parameters of the defect population. The resulting distributions can then be compared in terms of their mean values and their standard deviations.
- ✓ The effect of the defect size distribution on the fatigue strength: this can be examined by changing the parameters of the defect size distribution and fixing the other parameters (N, ρ and the volume of the samples).
- ✓ The effect of the spatial density of the pores on the fatigue strength by changing the parameter ρ and fixing the other parameters.
- ✓ The effect of the number of the samples (N) on the estimation of the fatigue strength.
- ✓ It is also possible to study different combinations of the aforementioned aspects.

In this paper, the modeling approach is firstly used to study the effect of the average defect size and the pore spatial density on the size effect and the scatter. The results are presented and discussed in the following paragraphs.

3. Sensitivity analyses: Effect of defect size distribution, pore density and number of samples on the fatigue strength predictions

3.1. Effect of the defect size distribution on the size effect and the scatter

As aforementioned, the first application of the model aims to simulate the effect of the average defect size on the size effect and the scatter of the fatigue strength. For this, two fictive defect populations that are very different in terms of their average defect size are used. The same defect density 'ρ' is used for both populations. In fact, 'Population 1' contains smaller defects when compared to 'Population 2' [Figure 9]. The parameters of the theoretical defect size distributions are summarized in Table 1.

Table 1 : Characteristics of the used fictitious populations of defects

	Lognormal distribution	
	μ	σ
Population 1	3	0.4
Population 2	5	0.3

where μ is the mean and σ is the standard deviation of the lognormal distribution.

These defect size distributions are visually presented in Figure 9.

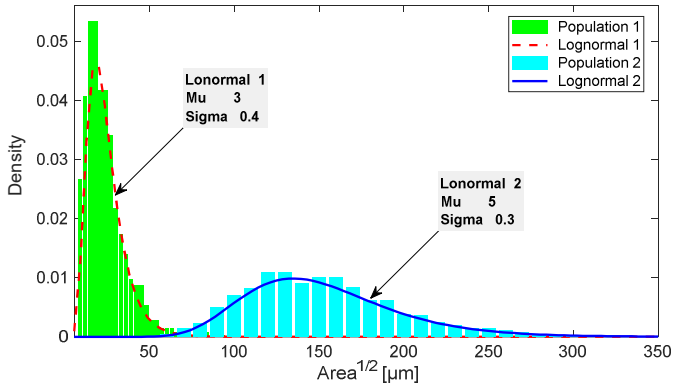

Figure 9 : The two fictive defect size populations investigated.

Using these two defect size populations, different sample volumes were generated. The sample height is held constant and the radius varies (see example in Figure 10). The parameters used for these simulation are :

- ρ =7 mm^{-3}
- h= 20 mm
- r: radius changes from 1 to 9 mm
- N=80 (numerical samples for each volume)
- The Fatigue Active Volume parameter is t=0.5 mm.

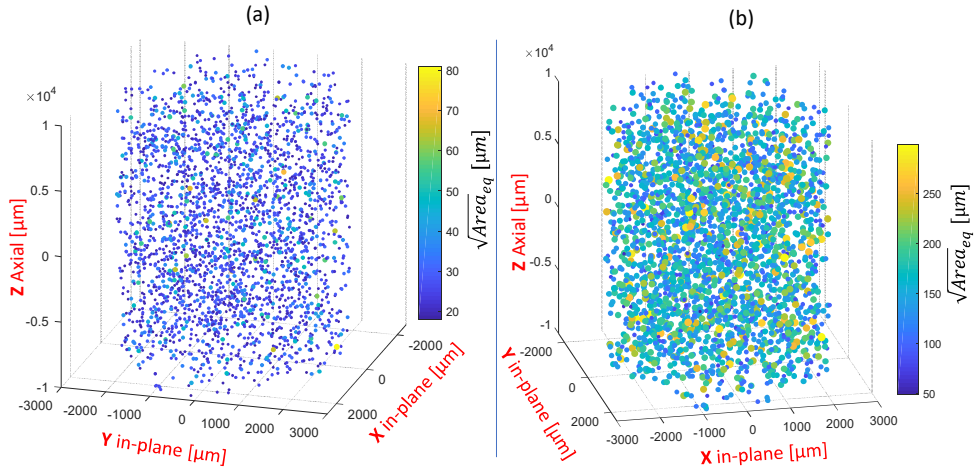

Figure 10 : Examples of numerical samples: (a) with population 1 and (b) with population 2.

The evolution of the critical defect size and the fatigue strength distributions as a function of the radius of the numerical samples are presented in Figure 11 and Figure 13 for both populations. The distributions are presented on lognormal probability plot. The comparison between the two populations is presented later.

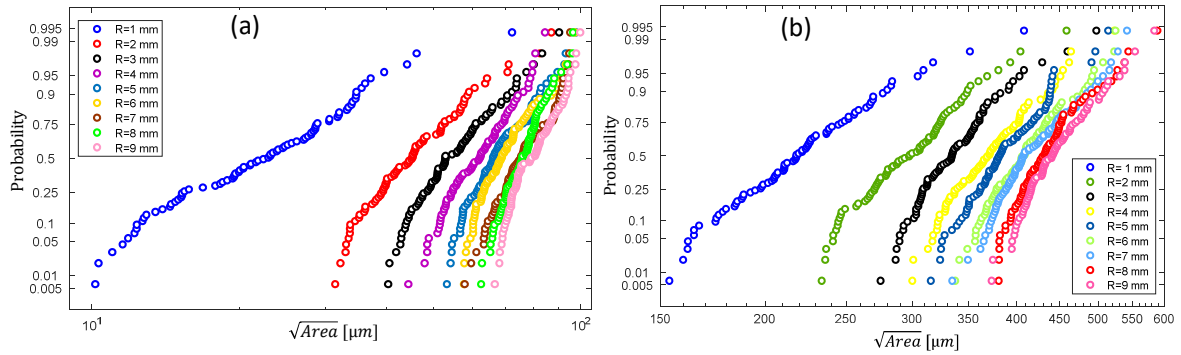

Figure 11: The critical defect size distributions for different sample radii for (a) Population 1 and (b) Population 2.

Figure 11 shows the evolution of the critical defect size distributions for different sample radii for the two populations. The results clearly show that the average size of the critical defect distributions increases when the sample radius is increased for both populations. This increase reaches a certain level where it stabilizes to a constant value. This stabilization indicates the presence of an RVE. The same conclusions can be extracted from Figure 12.

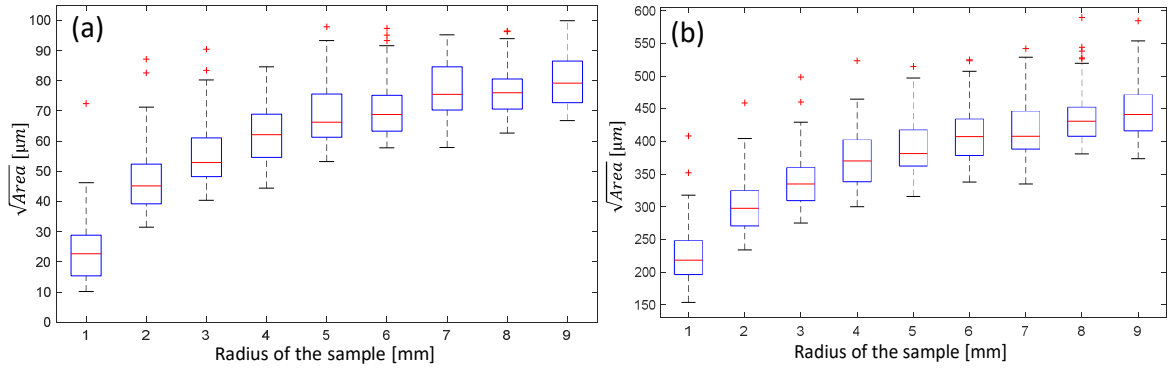

Figure 12: The evolution of the critical defect size as a function of the sample radius for (a) Population 1 and (b) Population 2. On each box, the central mark in red indicates the median, and the bottom and top edges of the box indicate the 25th and 75th percentiles, respectively, and the outliers are plotted individually using the '+' symbol.

Figure 13 shows the evolution of the fatigue strength distributions for different sample radii for both populations. It can be observed that by increasing the sample volume (or radius), the fatigue strength distribution decreases. This is the exact definition of the size effect. Furthermore, the decrease in the fatigue strength stabilizes at a certain volume that can be defined by the RVE. It should be noted that the saturation in the average critical defect size may occur at a different volume compared to the volume for which the saturation in terms of the fatigue strength occurs. This is because the relationship between the critical defect size and the fatigue strength is not linear.

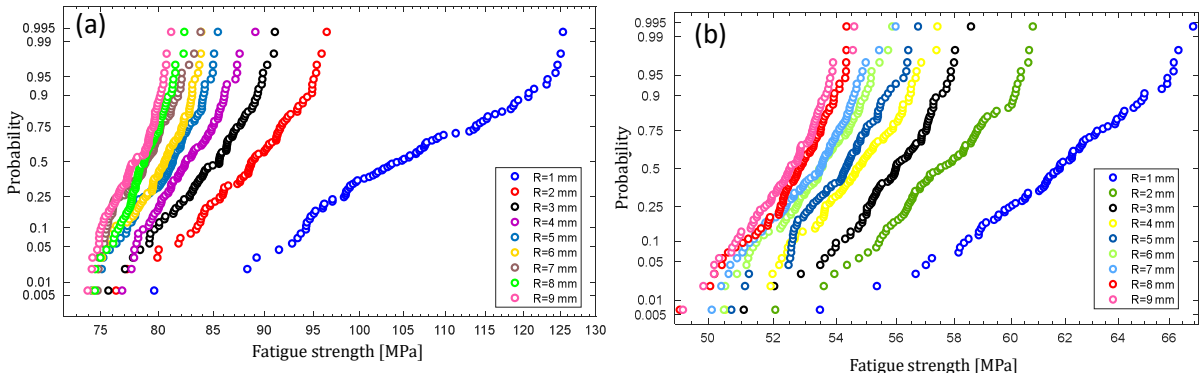

Figure 13: The evolution of the fatigue strength distributions for different sample radii for (a) Population 1 and (b) Population 2.

Besides the effect of the sample volume (or radius) on the fatigue strength, the Figure 14 gives insight into the change in the fatigue strength scatter when the sample volume (or radius is varied). It can be seen that the scatter is higher when the volume is small. Further analyses of the scatter are detailed in the following section.

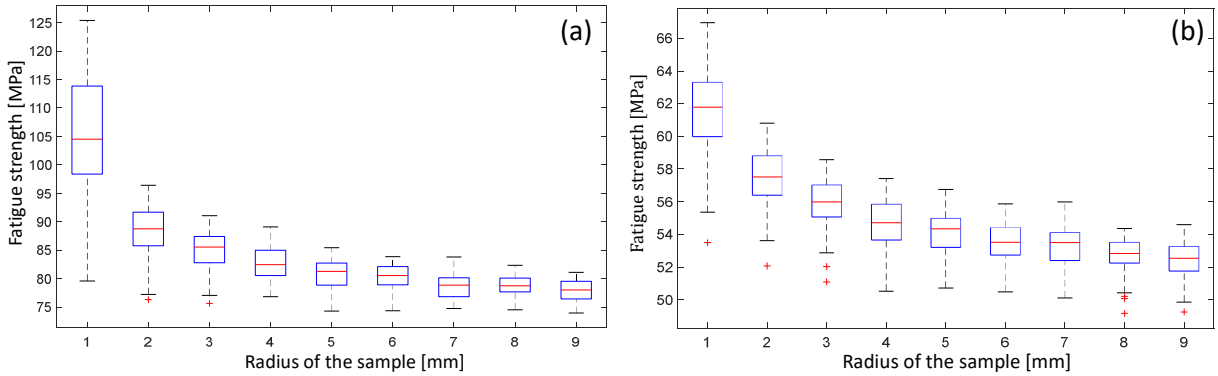

Figure 14: The evolution of fatigue strength as a function of the radius of the sample for (a) Population 1 and (b) Population 2.

Role of defect size population on the volume effect

As already stated, the main objective of this section of the article is to illustrate the effect of the defect population characteristics, in particular its average value, on the volume effect and the resulting scatter in the fatigue strength. Figure 15 shows the evolution of the average fatigue strength value as a function of the Fatigue Active Volume of the numerical samples. In the following sections, we have chosen to represent the results in terms of Fatigue Active volume as defined in Figure 3.

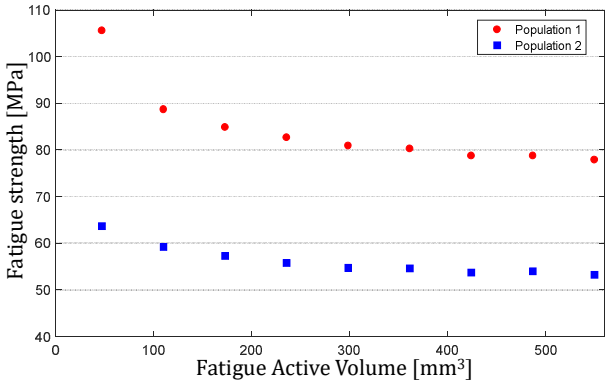

Figure 15: The evolution of fatigue strength as a function of the FAV for both populations.

- Firstly, both populations follow the same trend whereby the fatigue strength decreases with the sample volume.
- Secondly, the fatigue strength of the synthetic material with the defect population characterized by smaller defects (Population 1) is higher than the material where the defects are larger (Population 2).
- Thirdly, the decrease in the fatigue strength for Population 1 is more pronounced than the decrease for Population 2; this difference leads to the two materials having different volume effects. In fact, Population 1 shows a more pronounced volume effect compared to the Population 2 with the larger defects.
- Finally, for both populations the fatigue strength decreases and then tends to a stabilized value. This stabilization indicates the existence of a RVE for both materials. It can be seen that the RVE for Population 2 (with large defects) is smaller than the RVE for Population1 (with smaller defects). This can be explained by the fact that for Population 2 with larger defects, the transformation to the fatigue strength using the Kitagawa-Takahashi diagram occurs at the tail of the curve where the curve is relatively flat, leading to only a lower variation in the fatigue strength.

Role of the defect size population on the scatter of the fatigue strength

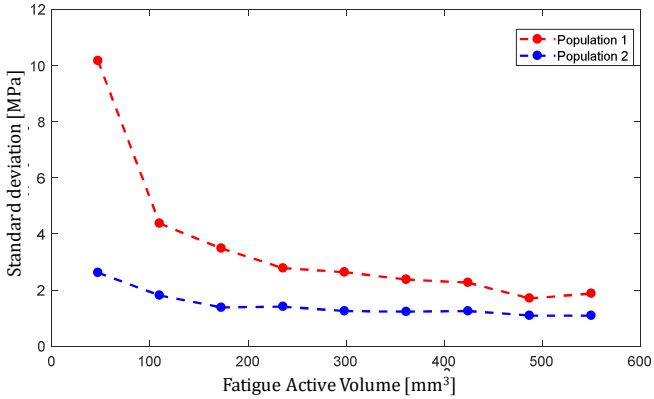

Figure 16: The standard deviation of the fatigue strength as a function of the Fatigue Active Volume

It is well known that fatigue data in the HCF regime is characterized by a high degree of scatter. Even if there are many attributes that contribute to this variability in the fatigue behavior, for cast aluminum alloys porosity is the principal factor affecting the fatigue scatter. In the present work, it is assumed that porosity is the only source of scatter in the fatigue strength.

Figure 16 presents the effect of the FAV on the scatter in the fatigue strength. From the results of the model, it can be noted that both populations show the same trend in the standard deviation of the fatigue strength. Secondly, the scatter in the fatigue strength is high for the smaller volumes and decreases with increasing sample volume. This result has already been demonstrated experimentally (El Khoukhi et al. 2019). Thirdly, the results show that Population 1 with smaller defects have higher scatter compared to Population 2 with larger defects. This result is in agreement with the experimental results obtained in by (El Khoukhi et al. 2019).

These results have been confirmed experimentally (El Khoukhi et al. 2019), for two different alloys with two different populations of defects. The results obtained on the studied alloys have been used for the validation of the proposed approach. The results of the validation will be presented and discussed in the section 4. However, firstly the effect of the pore spatial density on the fatigue behavior is investigated.

3.2. **Effect of the pore spatial density on the fatigue behavior**

The effect of the pore spatial density (Figure 17) on the fatigue strength is presented in this section. For this investigation, the following inputs to the probabilistic model must be defined:

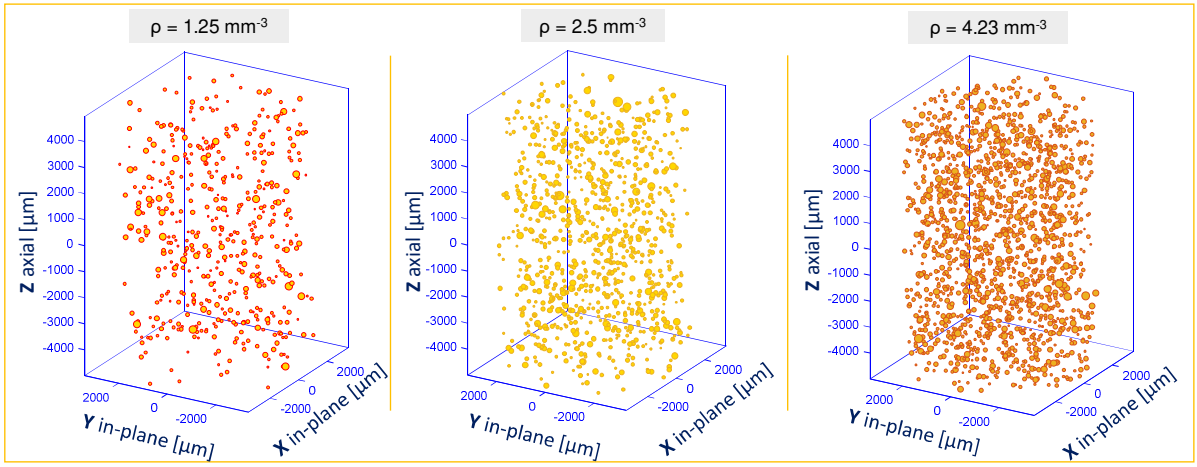

Figure 17: An example of three numerical samples with the same volume (FAV = 71 mm^3) but with different pore spatial densities.

- A single defect size distribution is used: lognormal distribution with µ=3 and σ=0.4
- The same spatial distribution is generated using the Poisson process
- 12 pore spatial densities (ρ) is used from 1 to 12 mm^{-3}
- 6 sample radii are used (R= 2000, 2500, 3000, 3100, 3300, 3500 [µm])
- For each calculation point, as a function of FAV and ρ (i.e. the red dots in Figure 18), the number of samples used to obtain the stabilization of the coefficient of variation is N=50 000. Therefore, for $12 \times 6 = 72$ calculation points, a total of 3.6 $x10^5$ samples were generated.

The effect of the pore spatial density (ρ) on the critical defect size is displayed in Figure 18. A higher pore density results in an increase of the average critical pore size (Figure 18. a) and leads to a decrease in the scatter of the critical pore size (Figure 18. b), for a fixed sample volume. The same behavior is observed in terms of the effect of the sample volume on the critical defect size distribution. Note that the scatter is presented in terms of the coefficient of variation, which is defined as the standard deviation divided by the average value. Physically, the effect of pore density on the critical defect size can be interpreted as when the overall number of pores in a given volume (sample size) increases, the size of the average critical defect increases. This is simply because many more large pores are available for crack initiation within the selected volume. Of course, when more large pores

are available for crack initiation, one would expect both the average fatigue strength and the fatigue strength scatter to be reduced. This is demonstrated in Figure 19.

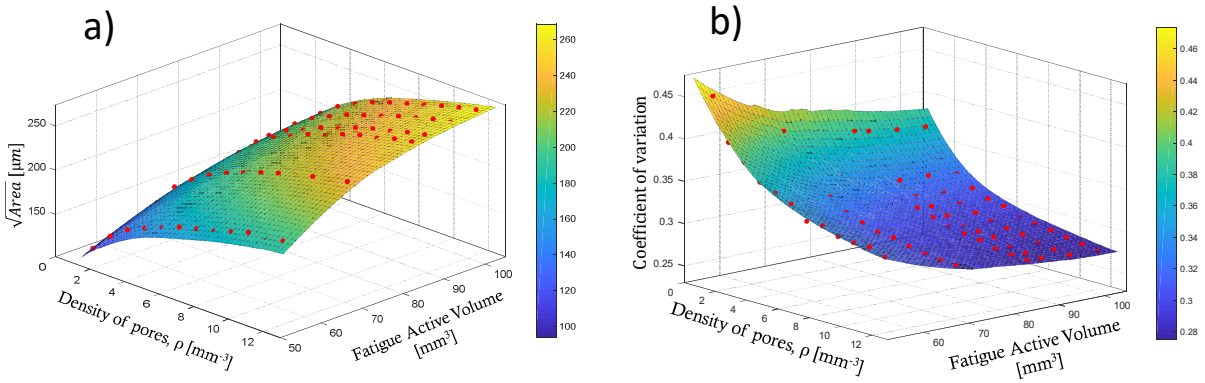

Figure 18: (a) The critical defect size as a function of the pore spatial density and the FAV. The red dots show the calculated values from which the surface is interpolated. (b) The coefficient of variation (standard deviation/mean) of the critical defects as a function of the pore spatial density and the FAV.

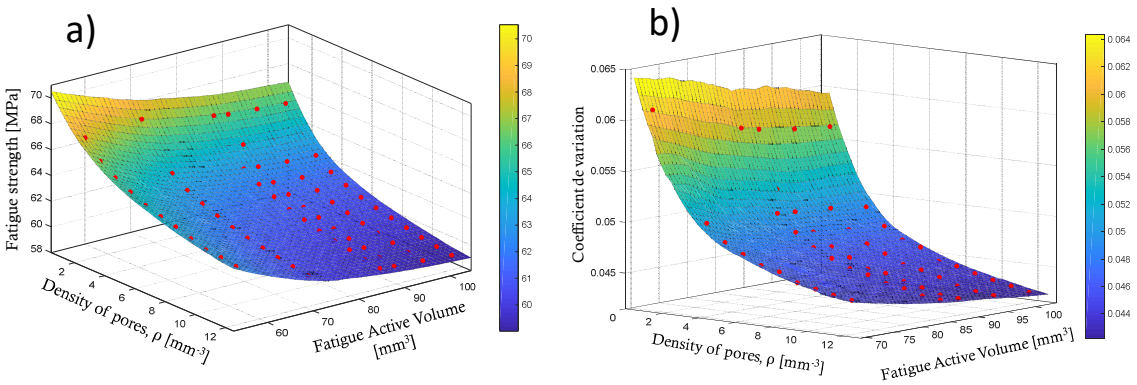

Figure 19: (a) The fatigue strength as a function of the pore spatial density and the FAV and (b) its coefficient of variation (standard deviation/mean).

Hence, the influence of the sample volume on the fatigue strength follows a similar trend to that of the pore density (ρ). The fatigue strength and its standard deviation are predicted to decrease with increasing specimen volume or pore density, and they tend towards almost constant values. This stabilization is predicted to happen at the RVE. From these results and the previous conclusions, it can be seen that the size of the RVE decreases:

- with increasing pore density (ρ).
- with an increasing average value of the defect size contained in the material.

3.3. **Effect of the number of samples on the fatigue strength prediction**

This approach can be extended to examine how changing certain parameters will affect the estimation of the fatigue strength. In the following, a sensitivity analysis of the effect of the number of samples on the estimated fatigue strength is presented. For this analysis, a constant sample volume is used, along with the characteristics of defect size distribution corresponding to an experimental alloy that we named alloy B and which we will present in detail in the following section. The only parameter that is varied is the number of samples N. The used parameters are the following:

- The defect size distribution for Alloy B: Generalized Extreme Value (k=0.35, σ=4.4, µ =22).
- The same spatial distribution is generated using the Poisson process
- One pore density value ρ=7 mm^{-3} is used
- One sample geometry is used (r=2.5 mm, h=12 mm)
- The number of samples N is varied (N= 5, 10, 20, 30, 40, 50, 60).

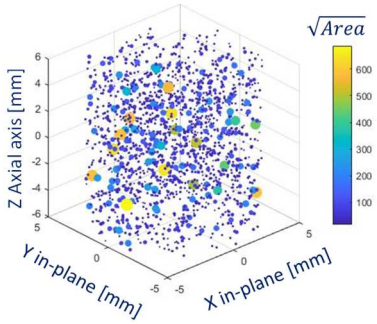

Figure 20: Geometry of the sample BV1 (r=2.5 mm, h=12 mm and ρ = 7 mm^{-3})

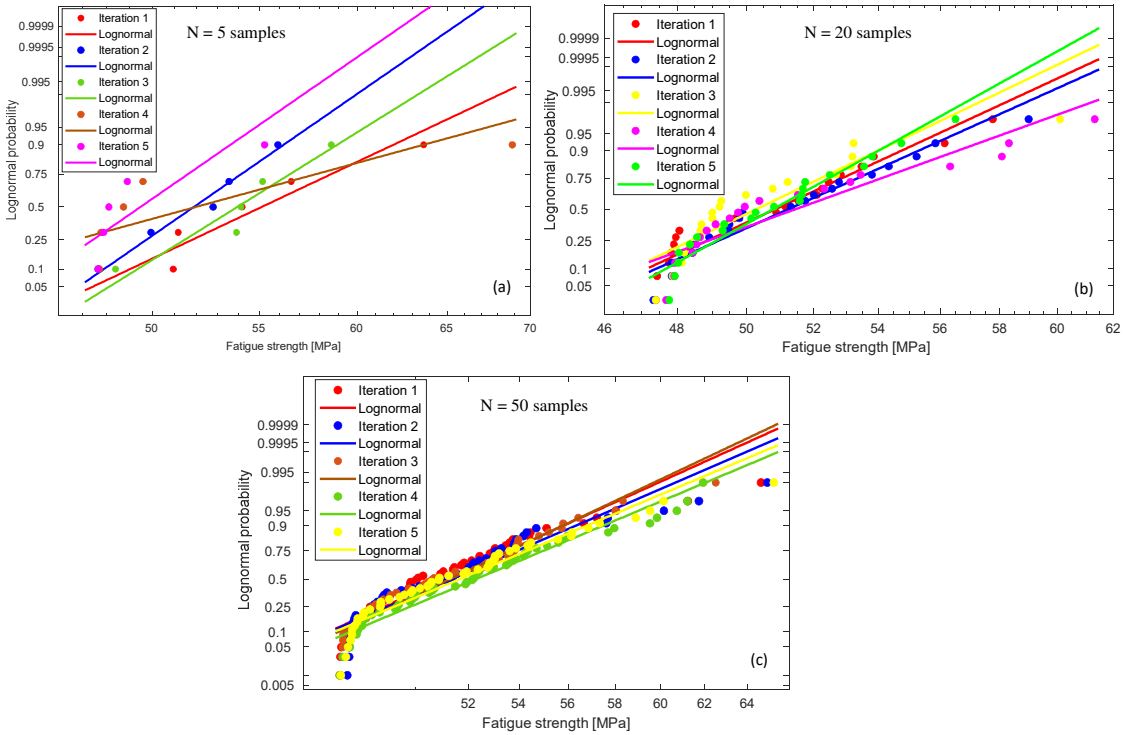

Figure 21: (a) Predicted fatigue strength distributions for N=5 samples, (b) for N=20, and (c) for N=50. The model has been repeated 5 times in each figure.

The Figure 21 shows the results for the analyses where the number of samples are: N=5, N=20 and N=50. The data is shown in the form of lognormal probability plots of the estimated fatigue strength distributions. In each figure, the analyses have been repeated five times for the same number of samples. The difference between the curves is due to the uncertainty in the estimation of the fatigue strength. This uncertainty depends on the number of the samples generated. We observe that when only 5 samples are used the results are unstable and five distinctly different distributions for the fatigue strength are obtained. However, as the number of samples that are generated is increased the stability increases and the distributions obtained via repeating the analysis 5 times converge.

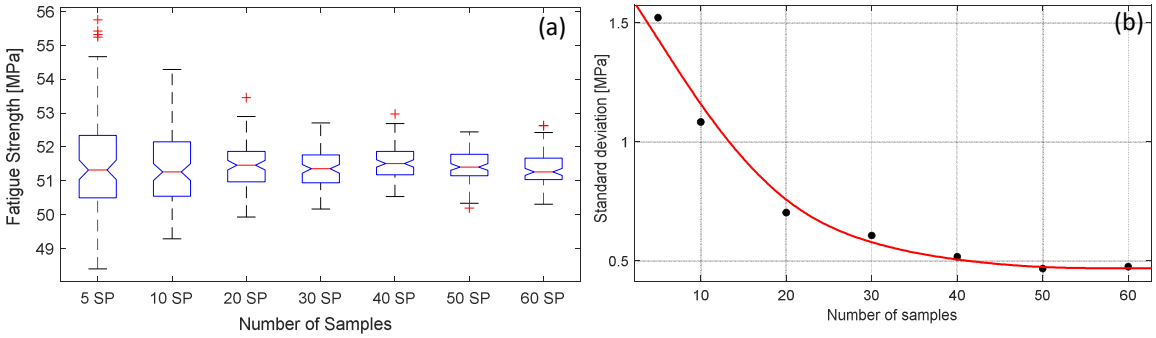

Figure 22: (a) Uncertainty in the estimation of the fatigue strength decreases as the number of samples increases, and (b) evaluation of the standard deviation of the fatigue strength. Here, the model has been repeated 100 iterations for each batch.

The evolution of the uncertainty as a function of number of samples is presented in Figure 22. It can be clearly seen that in order to obtain high precision in the estimation of the fatigue strength and its scatter a higher number of samples is necessary. For this sample volume and pore density (r=2.5 mm, h=12 mm and ρ = 7 mm^{-3}), with 100 iterations, stabilization is reached within N=50 samples (Figure 22 .b). It should be noted that the stabilized value of N depends on the sample volume and the pore density ρ. That means, if the numerical sample has a larger size, the stabilization will be reached with a lower number of samples N. In the same way, if the pore density ρ is higher in the numerical sample, the stabilization will be reached with a lower number of samples N. These results will be exploited to justify the choices (i.e. "N=50" and "number of iterations=100") made in the simulations presented in section 4 to compare the numerical and experimental results for the alloys being investigated.

4. Application to two cast aluminum alloys

In this section, the proposed model will be applied to two cast aluminum-silicon alloys that have been extensively studied from an experimental point of view (El Khoukhi et al. 2019; 2018). The objective is to investigate and validate the ability of the model to predict, for both alloys:

- the fatigue strength
- the scatter associated with the fatigue strength
- the sensitivity to size or volume effect (and implicitly stress gradient effect)
- size of the RVE in fatigue

4.1. Materials

To evaluate the capacity of the proposed approach to predict the influence of casting defects on the fatigue behavior, two primary cast aluminum alloys, referred to as alloys A [AlSi7Cu05Mg03-T7] and B [AlSi7Mg03-T7], have been used. These alloys were fabricated by different casting processes (alloy A: gravity die-casting and Alloy B: lost foam casting), and subject to the T7 heat treatment. These processes result in different porosity populations (i.e. pore density, defect size and spatial distribution…) and different mechanical properties. Previous work concerning the characterization of these materials has been done by (Le et al. 2016). Table 2, Table 3 and Table 4 summarize the mechanical and microstructural properties of these alloys.

Table 2: Chemical composition of the alloy A [AlSi7Cu0.5Mg0.3]

Element	Si	Cu	Mg	Zn	Mn	Ni	Ti	Pb	Fe	Sn
% in weight	6,5-7,5	0,4-0,6	0,28-0,4	<0,10	<0,10	<0,05	0,08-0,2	<0,05	<0,20	<0,05

Table 3: Chemical composition of the alloy B [AlSi7Mg0.3]

Element	Si	Cu	Mg	Zn	Mn	Ni	Ti	Pb	Fe	Sn
% in weight	6,5-7,5	<0,10	0,28-0,4	<0,10	<0,10	<0,05	0,08-0,2	<0,05	<0,20	<0,05

Table 4 : Properties of the investigated cast Al-Si alloys

	Alloy A	Alloy B
Designation	AlSi7Cu05Mg03 - T7	AlSi7Mg03 - T7
Casting Process	Gravity Die	Lost Foam
Heat treatment	T7	T7
SDAS (µm)	42±10	77±19
Young Modulus E (GPa)	77±6	68±5
Yield stress $\sigma_{Y0.2\%}$ (MPa)	260±2	240±5
Ultimate tensile strength σ_u (MPa)	304±4	251±6
Elongation A (%)	4.7±1.2	0.8±0.1
Void fraction (%)	0.03	0.28

An extensive experimental campaign involving 220 uniaxial fatigue tests with a load ratio of R=0.1, reported in (El Khoukhi et al. 2019; 2018) has highlighted the effect of casting defects on: (i) the size or volume effect, (ii) the scatter in the fatigue strength and (iii) and the RVE for these alloys. The experimental results are used here in order to validate the accuracy of the proposed probabilistic approach. As previously mentioned, certain material and model parameters must be provided so that the model can predict the fatigue behavior of the cast aluminum alloys. These parameters are:

- The defect size distribution in terms of $\sqrt{Area}_{eq}$
- The defect spatial distribution: characterization of the defect populations in these materials was presented in (El Khoukhi et al. 2020).
- The pore density ρ of each material.
- The specimen geometries.
- The number of the numerical samples generated (N)

It should be noted that the Kitagawa-Takahashi diagram used for these materials is the same diagram presented above in Figure 7.

Defect size distribution

Figure 23 shows the cumulative probability function of the defect size expressed in terms of $\sqrt{Area}_{eq}$ for the studied alloys. The data are obtained from 9 CT X-Rays scans with a total volume of V = 2.2×10^3 mm^3 for Alloy B and 4 CT X-Rays scans with total volume of V = 0.9×10^3 mm^3 for Alloy A. It can be seen that the maximum defect size for Alloy A is 285 µm and for Alloy B it is 1492 µm.

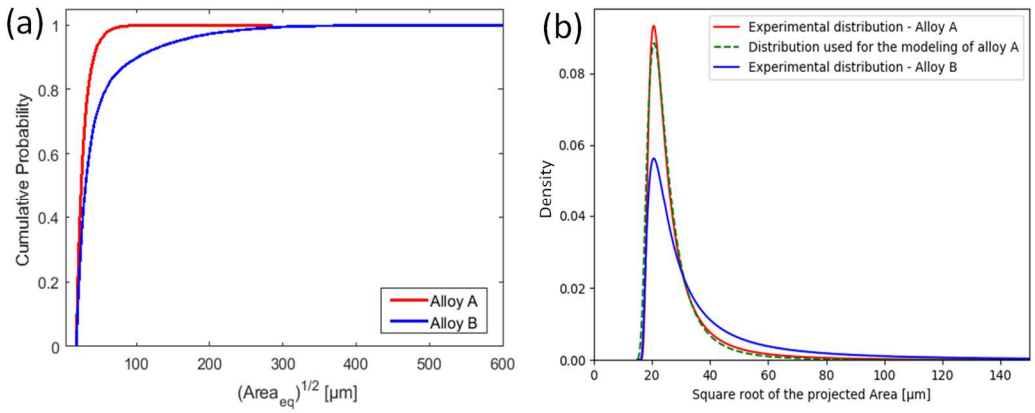

Figure 23: (a) Cumulative probability functions of the defect size distributions for (a) Alloy A and (b) Alloy B in terms of $\sqrt{Area}_{eq}$. (b) Probability density functions of the defect size distributions for Alloy A. The red curve is determined experimentally, and the green curve is its fit using the GEV distribution, and the blue one is for the alloy B.

In the previous work (El Khoukhi et al. 2020), we showed that the Generalized Extreme Value (GEV) distribution gives the highest value of the Ln likelihood. Hence, the GEV gives the best-fit for the defect size distribution for both alloys. The corresponding parameters are summarized in Table 6.

Spatial distribution

As discussed in (El Khoukhi et al. 2020), the Poison point process can be used to describe the spatial distribution of the defects in both alloys. The experimental analyses from the CT scans of the studied alloys indicate that the pore density for the Alloy A is ρ=13 mm^{-3} and for the Alloy B is ρ=7 mm^{-3}. These values will be used for the generation of the numerical samples. The total number of pores N_t contained in the generated numerical samples is given by (eq. 3).

Sample Geometries

In previous experimental work discussed in (El Khoukhi et al. 2019), different fatigue specimen geometries were defined, corresponding to different Fatigue Active Volumes. These are shown in Figure 24 and are referred to as: "V1-Small Volume", "V2-Reference Volume", "V3-Large Volume" and "VN2-Notched specimen". In order to compare the results of the model with the experimental results, the same sample volumes are generated numerically with similar defect populations [Figure 24, Figure 25, Figure 26, Figure 27 and Figure 28].

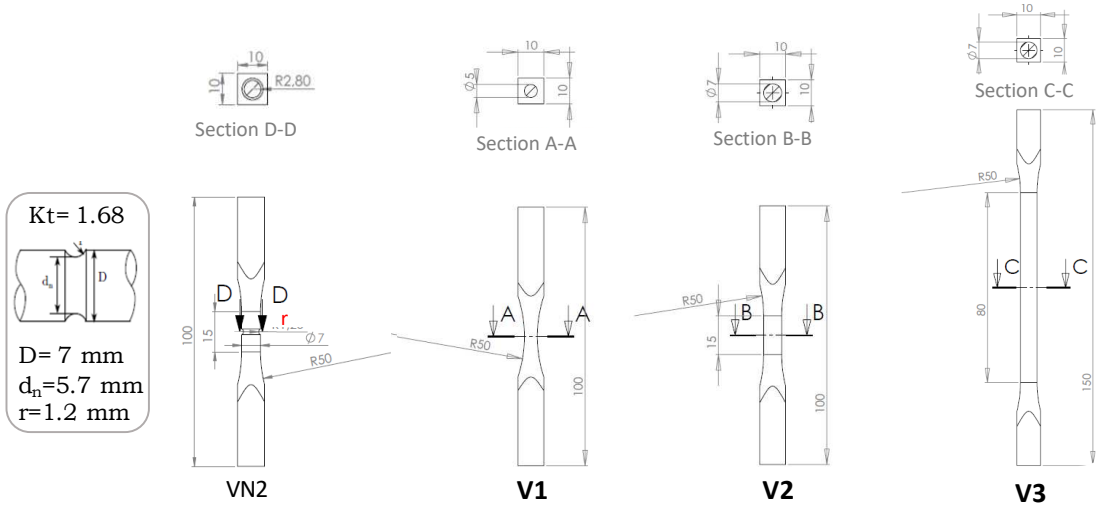

Figure 24: Sample geometries investigated experimentally (unit is mm) (El Khoukhi et al. 2019)

The following figures show examples of the generated numerical samples.

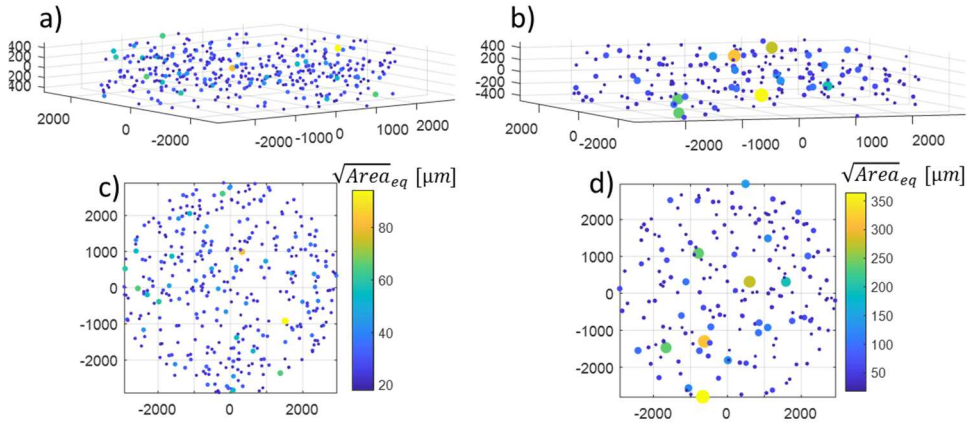

Figure 25: An example of a numerical sample for (a, c) Alloy A, Geometry "VN2-Notched specimen", Label "AVN2", and (b, d) Alloy B, Geometry "VN2-Notched specimen", label "BVN2". Dimensions are in µm.

For the sake of simplicity, for the notched samples, we consider the numerical volume to be cylindrical. In addition, the fatigue strength is expressed in terms of the local stress at the notch-tip.

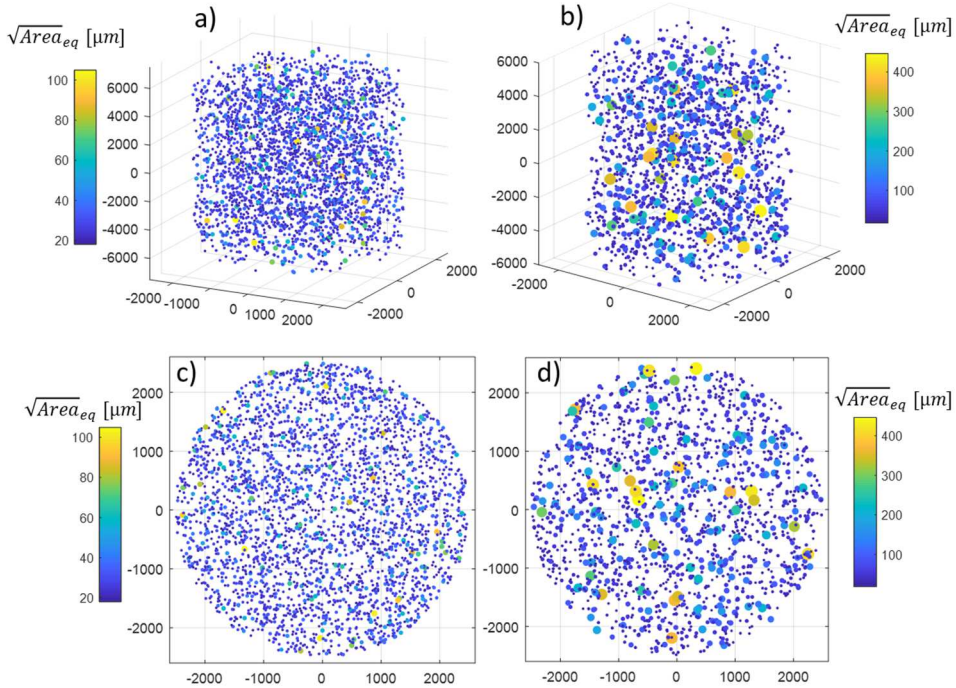

Figure 26: An example of a numerical sample for (a, c) Alloy A, Geometry "V1-Small Volume", Label "AV1", and (b, d) Alloy B, Geometry "V1-Small Volume, Label "BV1". Dimensions in µm.

Note that for the sake of simplicity the Geometry "V1-Small Volume", which experimentally has an hour-glass shaped, is considered to have a cylindrical shape for the numerical samples.

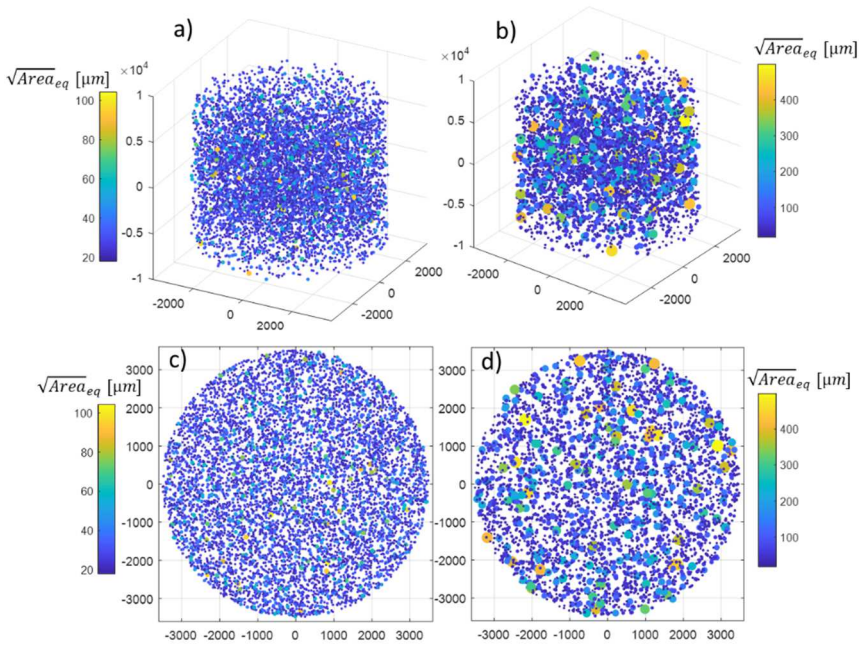

Figure 27: An example of a numerical sample for (a, c) Alloy A, Geometry "V2-Reference Volume", Label "AV2" and (b, d) Alloy B, Geometry "V2-Reference Volume", Label "BV2" (units in µm)

The third specimen geometry is "V3-Large Volume". This geometry was only tested experimentally for Alloy A, hence only numerical samples for Alloy A were generated.

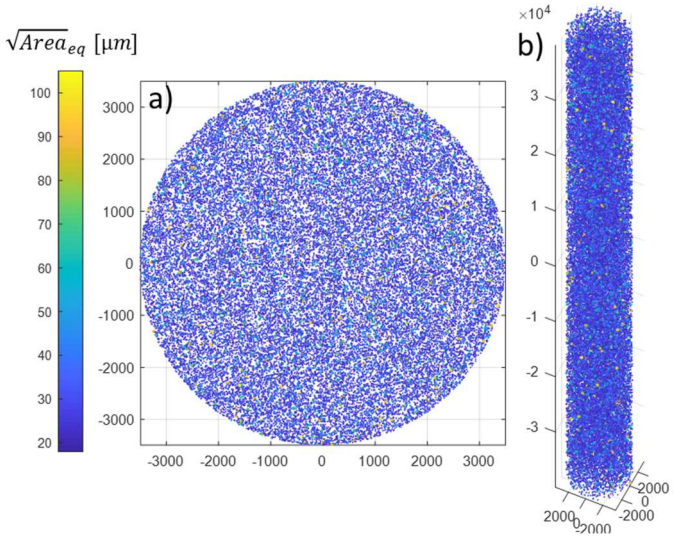

Figure 28: An example of a numerical sample for (a, b) Alloy A, Geometry "V3-Large Volume", Label "AV3" (units in µm).

Table 5: The characteristics of the samples used for the experimental work

Geometry	Number of specimens/samples		FAV_A in mm^3 for the sublayer of 500 µm	FAV_B in mm^3 for the sublayer of 650 µm
	Alloy A	Alloy B		
VN2	15	15	5	6
V1	24	9	90	110
V2	20	9	320	450
V3	9	0	912	-

Table 6: Summary of the model parameters and specimen geometries used to validate the proposed approach

	Alloy A	Alloy B
ρ: density of pores (mm^{-3})	13	7
Spatial distribution	Poisson process	Poisson process
Defect size distribution	Generalized Extreme Value (k=0.35, σ=4.4, μ =22)	Generalized Extreme Value (k=0.9, σ=9, μ =25)
Geometries investigated	AVN2, AV1, AV2, AV3	BVN2, BV1, BV2

where μ is the location parameter, σ is the scale parameter, and k is the shape parameter of the generalized extreme value distribution.

The other parameters used for the simulation are the number of numerical samples N=50 for each geometry/volume and 100 iterations are done in order to have a stabilized numerical distribution. An example shows that the stabilization is reached for the volume BV1 with the smallest pore density is examined in section 3.3.

4.2. **Validation of the probabilistic approach on experimental materials**

It this section the results are presented in terms of the estimated fatigue strength distributions. Firstly, the results for Alloy A are presented and discussed, followed by the results for Alloy B. It can be seen that the model provides a distribution of the fatigue strength for each volume. The average value of the resulting distribution and its standard deviation are compared to the experimental values for each alloy.

4.2.1.**Application to Alloy A**

Figure 29 shows the comparison between the proposed model and the experimental data for Alloy A with the notched geometry VN2 (labelled "AVN2").

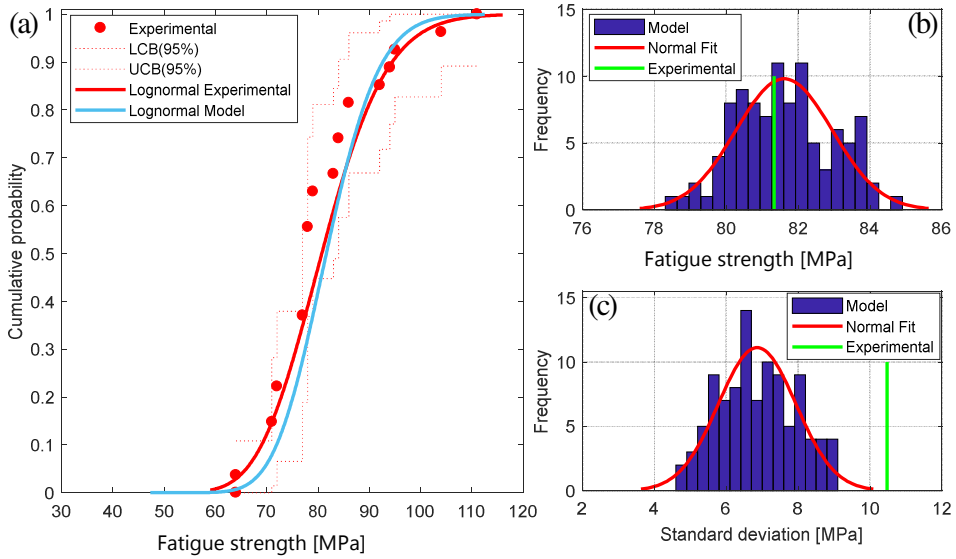

Figure 29: Comparison between the experimental data and the model predictions for AVN2

Figure 29(a) shows the experimental data in terms of the Cumulative Probability Function (CPF) fitted with the lognormal distribution and the predicted CPF. The results show good agreement between the predicted distribution and the experimental data as the predicted CPF is included in the 95% confidence interval of the experimental data. This result is confirmed by Figure 29(b) which shows that the experimental average fatigue strength is close to the average value of the numerical distribution. However, in terms of the scatter associated with this volume, the model predicts a lower

standard deviation compared to the experimental value [Figure 29(c)]. Further analyses of the difference between the numerical and the experimental data are presented later.

The same conclusions can be made for the AV1 and AV2 cases. The model results are in good agreement with the experimental results for the average value of the fatigue strength. However, the predicted scatter is low compared to the experimental data.

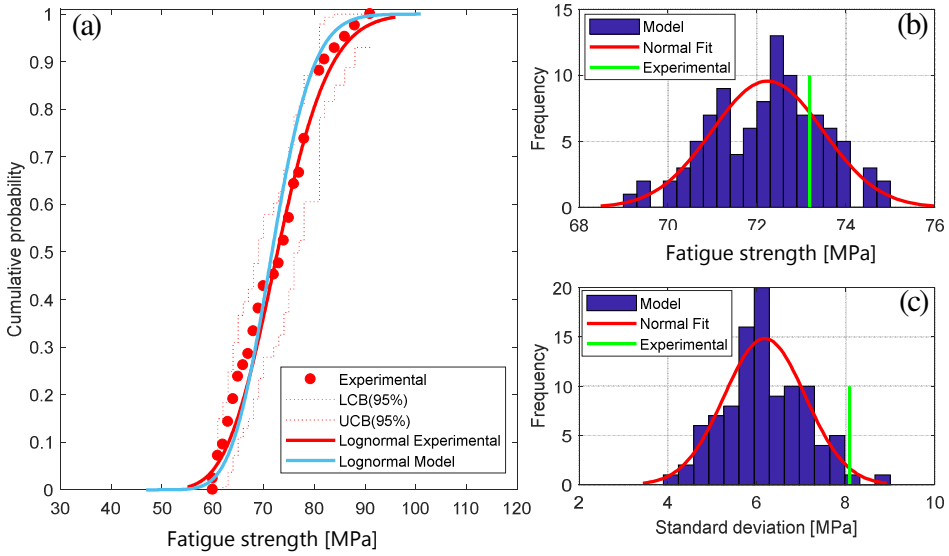

Figure 30: Comparison between the experimental data and the model predictions for AV1

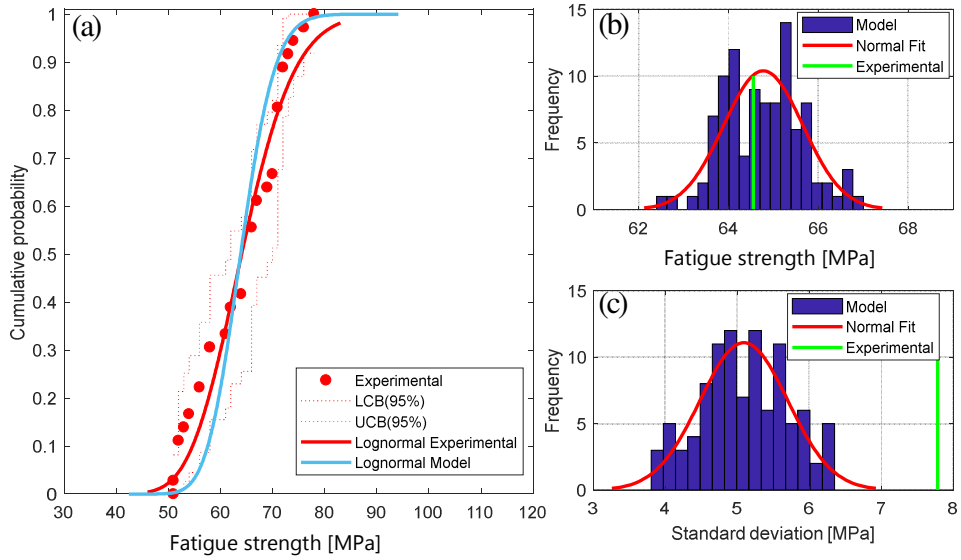

Figure 31: Comparison between the experimental data and the model predictions for AV2

For Alloy A and the geometry with the largest volume (AV3), the model gives an estimation of the average fatigue strength of 59 MPa and the experimental value is 62 MPa. Hence, the relative error is less than 5%. However, the scatter estimation is also underestimated, hence non conservative.

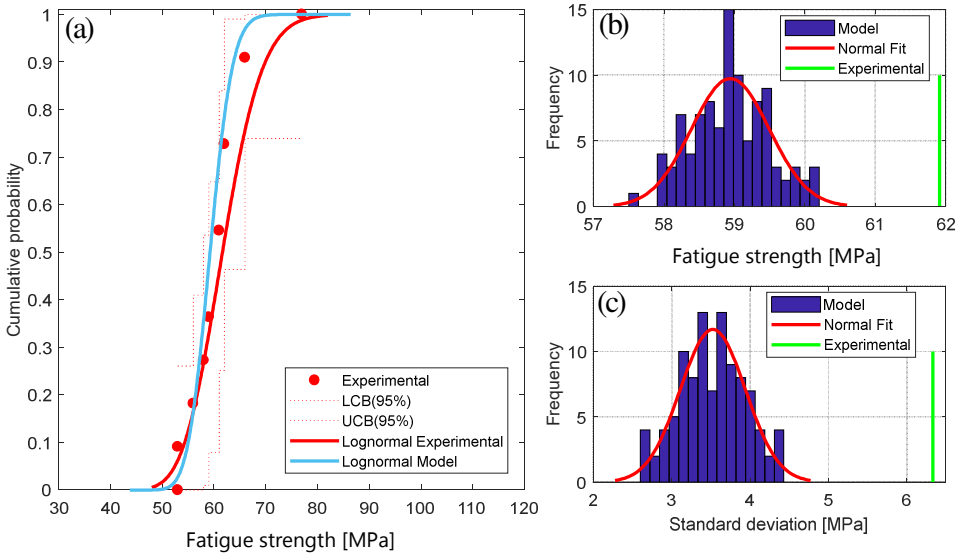

Figure 32: Comparison between the experimental data and the model predictions for AV3

A summary of the comparison between the experimental and the predicted data is shown in Table 7.

Table 7: Summary of the results for Alloy A

	Average fatigue strength [MPa]		Standard deviation [MPa]		Coefficient of Variation		Relative error = (Exp-Num)/Exp		
Batch	Exp.	Num.	Exp.	Num.	Exp.	Num.	Fatigue strength	Standard deviation	Coefficient of variation
AVN2	81.33	81.73	10.47	6.86	0.13	0.08	-0.005	0.35	0.35
AV1	73.19	72.25	8.09	6.00	0.11	0.08	0.013	0.26	0.25
AV2	64.56	64.81	7.78	5.02	0.12	0.08	-0.004	0.36	0.36
AV3	61.91	58.87	6.33	3.46	0.10	0.06	0.049	0.45	0.42

4.2.2. **Application to Alloy B**

In this section the proposed model is applied to Alloy B. The smooth specimen geometries (BV1 and BV2) and the notch specimen geometry (BVN2) are considered. In terms of the experimental data available for this material (El Khoukhi et al. 2019), it is considered that there are sufficient to accurately determine the average fatigue strengths, however, this is not the case for the scatter, especially when compared to Alloy A.

Concerning the prediction of the fatigue strength for Alloy B, the same conclusions can be drawn as those discussed above for Alloy A. It can be seen in Figure 33, Figure 34 and Figure 35 that good correlation is obtained between the experimental data and the model predictions for the fatigue strength distributions. The predicted CPFs are included in the 95% confidence intervals of the experimental data.

The predicted standard deviation for batch BVN2 is very close to the experimental value [Figure 33 (c)] and is lower for batches BV1 and BV2. The results are summarized in Table 8.

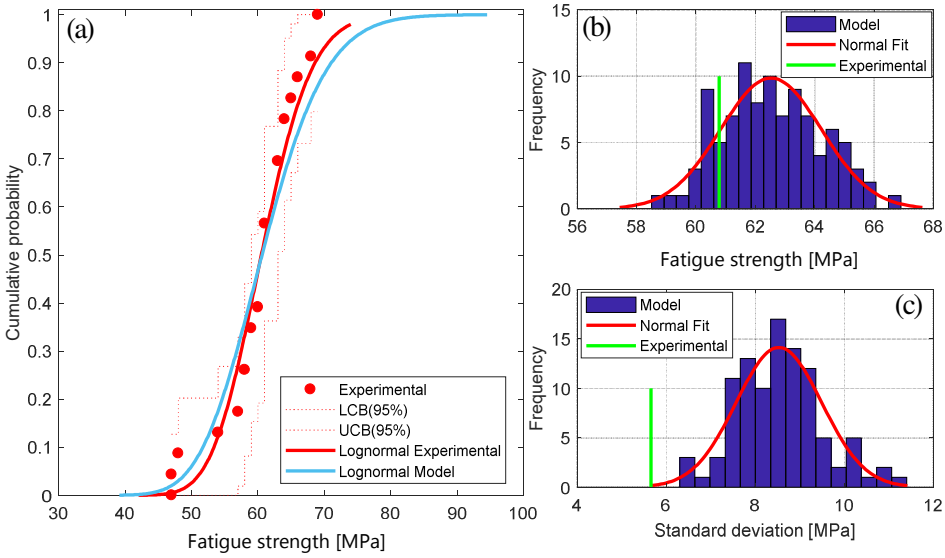

Figure 33: Comparison between the experimental data and the model predictions for BVN2

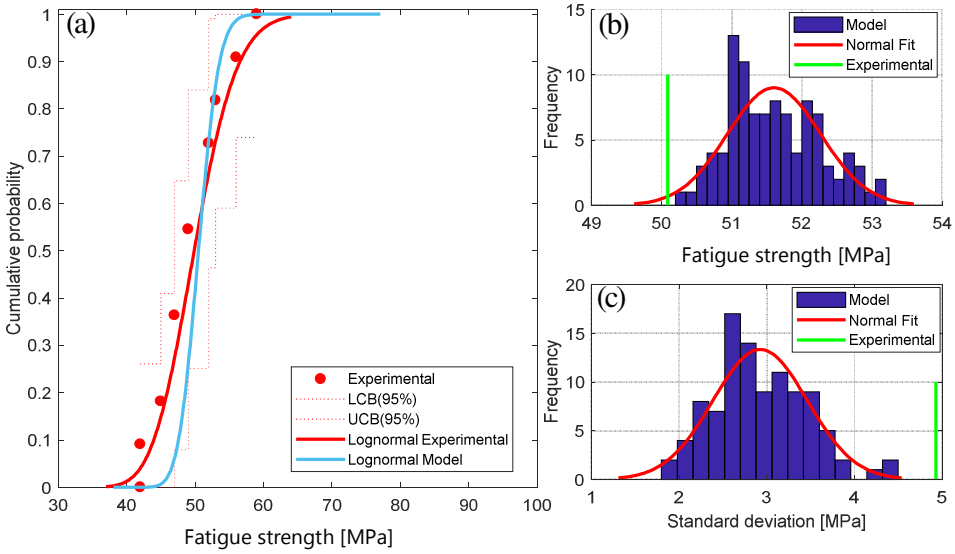

Figure 34: Comparison between the experimental data and the model predictions for BV1

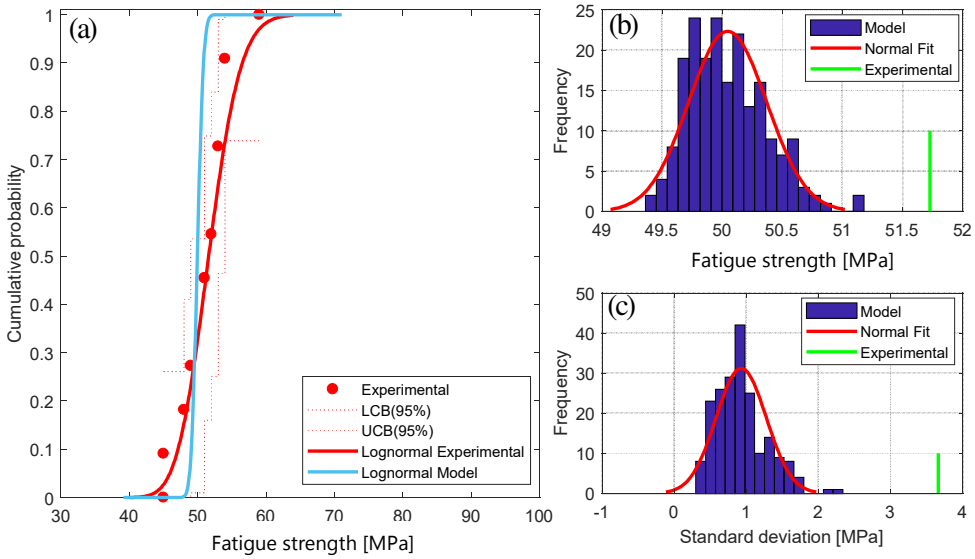

Figure 35: Comparison between the experimental data and the model predictions for BV2

Table 8: Summary of the results for Alloy B

	Average fatigue strength [MPa]		Standard deviation [MPa]		Coefficient of Variation		Relative error = (Exp-Num)/Exp		
Batch	Exp.	Num.	Exp.	Num.	Exp.	Num.	Fatigue strength	Standard deviation	Coefficient of variation
BVN2	60.78	60.27	5.66	7.10	0.09	0.12	0.01	0.25	0.27
BV1	50.09	51.22	4.93	3.11	0.10	0.06	0.02	0.37	0.38
BV2	51.73	50.17	3.66	1.09	0.07	0.03	0.03	0.70	0.69

It can be seen that the model accurately predicts the average fatigue strength with a relative error of less than 3% and results in a predicted standard deviation with the same order of magnitude as the experimental value. Note that for Alloy B, 9 specimens for batches BV1 and BV2 have been experimentally tested, and 15 for batch BVN2. For these batches, the estimation of the experimental standard deviation is not considered to be accurate, as a greater number of specimens are needed. Nevertheless, the predicted standard deviation is in general lower than the experimental values, except for batch BVN2.

4.2.3. **Summary on the prediction of fatigue strength and it scatter**

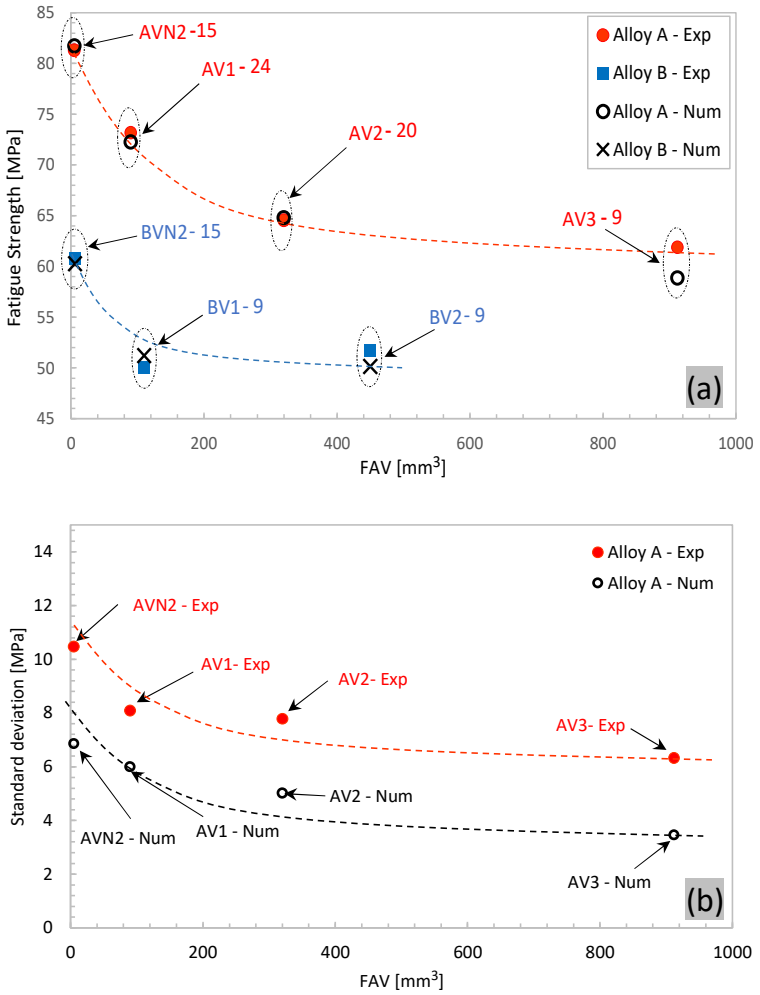

Figure 36: (a) Comparison between the experimental average fatigue strength and the corresponding predicted values for Alloys A and B versus the Fatigue Active Volume, and (b) the fatigue strength scatter for Alloy A versus the Fatigue Active Volume.

Figure 36 a. and Table 7 highlight that the proposed probabilistic approach is capable of predicting the high cycle fatigue strength of both alloys with a relative error less than 5%, including the accurate

prediction of the volume effect, for both smooth and notched geometries. Therefore, it can be concluded that the proposed model can be used:

- To evaluate the susceptibility of cast aluminum to the volume effect
- To predict their fatigue strength distribution
- To estimate the RVE in fatigue

In Figure 32 .b, we choose to represent only the data corresponding to the alloy A for which we have high number of samples. It can be seen that the proposed model is able to predict the experimental trend in terms of the influence of the Fatigue Active Volume on the standard deviation. That is the scatter is highest for small FAVs. However, the absolute values of the predicted standard deviation are consistently lower than the experimental values. This difference can be explained as follows.

It is well known that in the HCF regime the fatigue strength is characterized by high scatter which can be attributed to many sources. For the cast aluminum alloys investigated in this work, casting defects and in particular the presence of porosity are the principal source of scatter. Nevertheless, it is not the only factor influencing the scatter. Other sources could include experimental errors, environmental factors, residual stresses, microstructure, … . In the proposed model, it is assumed that the fatigue behavior is completely controlled by the porosity, which is the only source of dispersion. It is hence not surprising that the predicted standard deviations are systematically lower than the corresponding experimental values. In some cases, up to 2 times lower.

5. Discussion

It should be noted that the proposed probabilistic model assumes that the porosity controls the fatigue behavior of the material. This assumption is based on many experimental studies that showed that usually the fatigue failures were initiated from a pore close to the surface (El Khoukhi et al. 2019 ; Le et al. 2016 ; Rotella et al. 2017 ; Murakami 1991). The proposed method presents many advantages and some drawbacks. The advantages of the proposed model include:

- The average fatigue strength is predicted with high precision (relative error less than 5%).
- The trends in the fatigue strength scatter are correctly predicted, however the model underestimates the absolute values of the standard deviation associated with the fatigue strength.
- The RVE can be estimated.
- The size or volume effect can be investigated.
- Arbitrary geometries involving the presence of stress gradients can be investigated through the definition of the Fatigue Active Volume (FAV).
- The model can be used to assess the variability due to the manufacturing process and the effect of the process parameters on the fatigue behavior of the alloys.
- For information, the computational time on a numerical volume AV2 and N=50 and 100 iterations is almost 12 min 22 s. The simulation was conducted on computer with a Processor Intel® Core™ i3-8145U CPU@2.10GHz with 8 Gbytes of RAM.

The proposed model has the following limits and drawbacks:

- The model is well suited to material for which the fatigue behavior is controlled by the presence of “well defined” defects such as micro-shrinkage porosity in cast materials. Its application to other defect types or microstructural heterogeneities, such as inclusions or persistent slip bands, is possible but should be validated experimentally.
- The model assumes that porosity is the only source of scatter. Hence it underestimates the scatter.
- The casting defects are considered to be perfectly spherical. This assumption seems to be valid for the case of cast aluminum alloys, but it may not be appropriate for Titanium alloys or Steels. For different materials and alloys, the general framework should not be changed, however modeling of the local fatigue strength should be revised to take into account the variability due to the morphology of the defects. If there is indeed an effect of the morphology, its characterization in relation to the defect size must be performed. Random sampling of the defect orientation and

aspect ratio could be included in the modelling approach. Some work has been carried out by other authors to take in account the defect shape in cyclic loading, for example (Mbiakop, Constantinescu, and Danas 2015).

- This approach is valid only when the failure mechanism is a pore (or an oxide).
- In order to consider the scatter observed in Figure 7, instead of considering a deterministic Kitagawa-Takahashi diagram, a probabilistic Kitagawa-Takahashi diagram could have been defined. However, it should be noted that even though this was not done here, the predictions are accurate. In this work, we voluntarily chose to use a deterministic Kitagawa-Takhashi diagram and to describe the variability only by the defect size and their spatial distribution. The results show that a major part of the scatter is caused by the variability of the defect size.
- The approach presented in this study could be applied in an industrial context, as long as the Kitagawa-Takahashi Diagram corresponding to the service loading conditions of the component (defined by the load ratio R and the multiaxiality) is known. A possible way of doing this was proposed by (Le et al. 2016) for different cast aluminum alloys.

6. Conclusions

In this work, a probabilistic approach to model the uniaxial fatigue strength with a load ratio of R=0.1 has been established. It allows to investigate the statistical characteristics of the fatigue strength controlled by the porosity population in cast aluminum alloys. The results show that the average pore size, the pore density, and the specimen volume, all influence the fatigue strength of these alloys. In general, the largest pore that is close to the free surface determines the fatigue strength. The average value and standard deviation of the fatigue strength decrease with increasing average pore size, and pore density. The specimen volume was also found to influence the fatigue strength by affecting the number of pores and their proximity with the specimen surface, this result explains the size effect phenomenon. The characteristics of the parent defect population are found to control the magnitude of the size effect. In fact, a population of defects with a smaller size leads to a high size effect and high scatter in the fatigue strength compared to a defect population with larger defect sizes.

By applying the model to two cast aluminum alloys, it is demonstrated that the predicted fatigue strength is in excellent agreement with the experimental results. Hence, it is concluded that the model can be used to:

- predict the fatigue strength distribution for smooth and notched geometries, via the definition of the Fatigue Active Volume (FAV)
- evaluate the volume effect
- estimate the RVE in fatigue
- estimate the trends in terms of the scatter (but underestimates the scatter)

The principal drawbacks and limits of the model are:

- that it assumes that the fatigue behavior is completely controlled by porosity. Hence, it may not be suitable for all materials with different fatigue damage mechanisms.

Acknowledgments

The authors gratefully acknowledge the financial support of the OPENLAB Materials and Processes, and the French National Agency for Research and Technology (ANRT)

References

Ai, Y., S. P. Zhu, D. Liao, J. A. F. O. Correia, C. Souto, A. M. P. De Jesus, and B. Keshtegar. 2019. "Probabilistic Modeling of Fatigue Life Distribution and Size Effect of Components with Random Defects." *International Journal of Fatigue* 126 (September): 165–73. https://doi.org/10.1016/j.ijfatigue.2019.05.005.

Ai, Yang, Shun-Peng Zhu, Ding Liao, José A. F. O. Correia, Abílio M. P. De Jesus, and Behrooz Keshtegar. 2019. "Probabilistic Modelling of Notch Fatigue and Size Effect of Components Using Highly Stressed Volume Approach." *International Journal of Fatigue* 127 (October): 110–19. https://doi.org/10.1016/j.ijfatigue.2019.06.002.

Boromei, I, L Ceschini, Al Morri, An Morri, G Nicoletto, and E Riva. 2010. "Influence of the Solidification Microstructure and Porosity on the Fatigue Strength of Al-Si-Mg Casting Alloys" 28: 7.

Devlukia, J., G. Bargmann, and I. Rüstenberg. 1997. "Fatigue Assessment of an Automotive Suspension Component Using Deterministic and Probabilistic Approaches." In *European Structural Integrity Society*, edited by G. Marquis and J. Solin, 22:1–16. Fatigue Design of Components. Elsevier. https://doi.org/10.1016/S1566-1369(97)80003-9.

El Haddad, M. H., T. H. Topper, and K. N. Smith. 1979. "Prediction of Non Propagating Cracks." *Engineering Fracture Mechanics* 11 (3): 573–84. https://doi.org/10.1016/0013-7944(79)90081-X.

El Khoukhi, Driss, Franck Morel, Nicolas Saintier, Daniel Bellett, and Pierre Osmond. 2018. "The Effect of Microstructural Heterogeneities on the High Cycle Fatigue Scatter of Cast Aluminium Alloys: From an Elementary Volume to the Structure." Edited by G. Hénaff. *MATEC Web of Conferences* 165: 14006. https://doi.org/10.1051/matecconf/201816514006.

El Khoukhi, Driss, Franck Morel, Nicolas Saintier, Daniel Bellett, Pierre Osmond, and Viet-Duc Le. 2020. "Spatial Point Pattern Methodology for the Study of Pores 3D Patterning in Two Casting Aluminium Alloys," 2020.

El Khoukhi, Driss, Franck Morel, Nicolas Saintier, Daniel Bellett, Pierre Osmond, Viet-Duc Le, and Jérôme Adrien. 2019. "Experimental Investigation of the Size Effect in High Cycle Fatigue: Role of the Defect Population in Cast Aluminium Alloys." *International Journal of Fatigue* 129 (December): 105222. https://doi.org/10.1016/j.ijfatigue.2019.105222.

Engelke, Torben, and Alfons Esderts. 2018. "Analytical Strength Assessments of Austempered Ductile Iron Components," 5.

Freudenthal, A. M., and Herbert John Gough. 1946. "The Statistical Aspect of Fatigue of Materials." *Proceedings of the Royal Society of London. Series A. Mathematical and Physical Sciences* 187 (1011): 416–29. https://doi.org/10.1098/rspa.1946.0086.

Gaenser, Hans-Peter. 2008. "Some Notes on Gradient, Volumetric and Weakest Link Concepts in Fatigue." *Computational Materials Science* 44 (2): 230–39. https://doi.org/10.1016/j.commatsci.2008.03.021.

Iben Houria, Mohamed, Yves Nadot, Raouf Fathallah, Matthew Roy, and Daan M. Maijer. 2015. "Influence of Casting Defect and SDAS on the Multiaxial Fatigue Behaviour of A356-T6 Alloy Including Mean Stress Effect." *International Journal of Fatigue* 80 (November): 90–102. https://doi.org/10.1016/j.ijfatigue.2015.05.012.

Kloos, K. H., A. Buch, and D. Zankov. 1981. "Pure Geometrical Size Effect in Fatigue Tests with Constant Stress Amplitude and in Programme Tests." *Materialwissenschaft Und Werkstofftechnik* 12 (2): 40–50. https://doi.org/10.1002/mawe.19810120205.

Kuguel, R. 1961. "A Relation between Theoretical Stress Concentration Factor and Fatigue Notch Factor Deduced from the Concept of Highly Stressed Volume." *ASTM Proc.* 61: 732–48.

Lanning, David B., Theodore Nicholas, and George K. Haritos. 2005. "On the Use of Critical Distance Theories for the Prediction of the High Cycle Fatigue Limit Stress in Notched Ti–6Al–4V." *International Journal of Fatigue* 27 (1): 45–57. https://doi.org/10.1016/j.ijfatigue.2004.06.002.

Le, Viet-Duc, Franck Morel, Daniel Bellett, Nicolas Saintier, and Pierre Osmond. 2016. "Multiaxial High Cycle Fatigue Damage Mechanisms Associated with the Different Microstructural

Heterogeneities of Cast Aluminium Alloys." *Materials Science and Engineering: A* 649 (January): 426–40. https://doi.org/10.1016/j.msea.2015.10.026.

Lipp, K., J. Baumgartner, and P. Beiss. 2013. "Fatigue Design of Sintered Steel Components: Effect of Stress Concentrations and Mean Stresses on Local Strength Using Highest Stressed Volume Approach." *Powder Metallurgy* 56 (5): 337–41. https://doi.org/10.1179/0032589913Z.000000000141.

Morel, Franck, and Thierry PALIN-LUC. 2002. "A Non-Local Theory Applied to High Cycle Multiaxial Fatigue." *Fatigue & Fracture of Engineering Materials & Structures* 25 (7): 649–65. https://doi.org/10.1046/j.1460-2695.2002.00527.x.

Mu, P., Y. Nadot, C. Nadot-Martin, A. Chabod, I. Serrano-Munoz, and C. Verdu. 2014. "Influence of Casting Defects on the Fatigue Behavior of Cast Aluminum AS7G06-T6." *International Journal of Fatigue* 63 (June): 97–109. https://doi.org/10.1016/j.ijfatigue.2014.01.011.

Murakami, Y., and M. Endo. 1994. "Effects of Defects, Inclusions and Inhomogeneities on Fatigue Strength." *International Journal of Fatigue* 16 (3): 163–82. https://doi.org/10.1016/0142-1123(94)90001-9.

Murakami, Yukitaka. 1991. "Effects of Small Defects and Nonmetallic Inclusions on the Fatigue Strength of Metals." Key Engineering Materials. Trans Tech Publications Ltd. 1991. https://doi.org/10.4028/www.scientific.net/KEM.51-52.37.

Papadopoulos, Ioannis V., and Vassilis P. Panoskaltsis. 1996. "Invariant Formulation of a Gradient Dependent Multiaxial High-Cycle Fatigue Criterion." *Engineering Fracture Mechanics* 55 (4): 513–28. https://doi.org/10.1016/S0013-7944(96)00047-1.

Pollak, Randall D. 2005. "Analysis of Methods for Determining High Cycle Fatigue Strength of a Material with Investigation of Titanium-Aluminum-Vanadium Gigacycle Fatigue Behavior." http://adsabs.harvard.edu/abs/2005PhDT.....271P.

Rafsanjani, Hesam Mirzaei, and John Dalsgaard Sørensen. 2015. "Reliability Analysis of Fatigue Failure of Cast Components for Wind Turbines." *Energies* 8 (4): 2908–23. https://doi.org/10.3390/en8042908.

Romano, Simone, Stefano Beretta, Stefano Miccoli, and Michael Gschweitl. 2019. "Probabilistic Framework for Defect Tolerant Fatigue Assessment of AM Parts Applied to a Space Component." *ASTM International*, April.

Rotella, A., Y. Nadot, M. Piellard, and R. Augustin. 2017. "Influence of Natural Defects on the Fatigue Limit of a Cast Al-Si Alloy." *Procedia Structural Integrity*, 3rd International Symposium on Fatigue Design and Material Defects, FDMD 2017, 7 (January): 513–20. https://doi.org/10.1016/j.prostr.2017.11.120.

Serrano-Munoz, Itziar, Jean-Yves Buffiere, Rajmund Mokso, Catherine Verdu, and Yves Nadot. 2017. "Location, Location & Size: Defects Close to Surfaces Dominate Fatigue Crack Initiation." *Scientific Reports* 7 (March): 45239.

Shirani, M., and G. Härkegård. 2011. "Fatigue Life Distribution and Size Effect in Ductile Cast Iron for Wind Turbine Components." *Engineering Failure Analysis* 18 (1): 12–24. https://doi.org/10.1016/j.engfailanal.2010.07.001.

Sonsino, C. M., and G. Fischer. 2005. "Local Assessment Concepts for the Structural Durability of Complex Loaded Components." *Materialwissenschaft Und Werkstofftechnik* 36 (11): 632–41.

Sun, Chengqi, and Qingyuan Song. 2018. "A Method for Predicting the Effects of Specimen Geometry and Loading Condition on Fatigue Strength." *Metals* 8 (October): 811. https://doi.org/10.3390/met8100811.

Weibull, Waloddi. 1939. *The Phenomenon of Rupture in Solids,*. Stockholm: Generalstabens litografiska anstalts förlag.

Yi, J.Z., X. Zhu, J.W. Jones, and J.E. Allison. 2007. "A Probabilistic Model of Fatigue Strength Controlled by Porosity Population in a 319-Type Cast Aluminum Alloy: Part II. Monte-Carlo Simulation." *Metallurgical and Materials Transactions A* 38 (5): 1123–35. https://doi.org/10.1007/s11661-006-9069-2.

Zhu, Shun-Peng, Stefano Foletti, and Stefano Beretta. 2018. "Evaluation of Size Effect on Strain-Controlled Fatigue Behavior of a Quench and Tempered Rotor Steel: Experimental and Numerical Study." *Materials Science and Engineering: A* 735 (September): 423–35. https://doi.org/10.1016/j.msea.2018.08.073.